Table 2. **Effects of quinone-binding site inhibitors on SQR activity of *P. y. yoelii* mitochondria.**

100 μM inhibitor	*P. y. yoelii* mitochondria	Rat liver mitochondria
Control	100%	100%
Atpenin A5	<0.4	<0.05
Carboxin	<0.4	<0.05
Flutoranil	58	22
TTFA	80	12
HQNO	54	94
Plumbagin	52	98
DNP-17	67	99

Control activities (mean ± SD) were 2.66 ± 0.02 (*P. y. yoelii*) and 180 ± 5 (rat liver) mU/mg protein.

forward reaction of TCA cycle (i.e. the oxidation of succinate). It should be noted that *Plasmodium* complex II was more resistant to known quinone-binding site inhibitors for mammalian complex II (Table 2), probably due to the divergence of membrane anchor subunits of *Plasmodium* complex II.

From the whole cell lysate of *P. falciparum*, Suraveratum *et al.* (*28*) purified complex II as the Fp/Ip heterodimer with an apparent molecular weight of 90 kDa and claimed that it has a much lower K_m value (3 μM) for succinate and plumbagin-sensitive SQR activity. However, the concentration (0.2%) of octyl glucoside used for the isolation of *P. falciparum* complex II was not enough for the solubilization of membrane proteins (i.e. critical micell concentration of octyl glucoside is 0.73%). Octyl glucoside likely dissociates the Fp/Ip dimer from the membrane anchor and the aerobic isolation of the Fp/Ip dimer would damage the iron–sulphur clusters in Ip. Thus, SQR activity of such preparations need to be carefully examined.

Plasmodium CybL and CybS are still not annotated in the current database (*6*, *7*), likely due to the divergence from ortholog sequences. However, 2D–PAGE analysis (Fig. 3), SQR activity (Fig. 1, refs. *20*, *25*) and the structure of quinone-binding site in complex II (*30–32*) support the presence of these membrane anchor subunits in *Plasmodium* spp. In membrane anchors of complex II, "$Rx_{16}Sx_2HR$" (helix I) and '$YHx_{10}D$' (helix II) motifs in CybL and '$LHx_{10}DY$' (helix II) motif in CybS are conserved for quinone/haem binding. And only such motifs are conserved in protist membrane anchors (*45*). One candidates for *P. y. yoelii* CybL (accession no. XP_731082, 10,086 Da) and one candidate for CybS (accession no. XP_726783, 10,379 Da) can be identified from 3,310 ORFs shared by *P. falciparum* and *P. y. yoelii* on the basis of the size (<200 amino acid residues), the presence of transmembrane segments (≤3), and the quinone/haem-binding motifs. PyCybL and PyCybS have two transmembrane regions and contain the quinone/haem-binding motifs, '$Rx_{14}Sx_2HY$' and '$YYx_{10}DY$' motifs and '$Yx_{10}G$' motif, respectively. In *S. cerevisiae* strain S288C (Baker's yeast), CybS (accession no. NP_010463) uses the $Yx_{10}DY$ motif, and the His-to-Tyr mutant of the CybL $YHx_{10}D$ motif retained a half of the enzyme activity and haem (*46*). Thus, in *Plasmodium* CybL and CybS, Tyr could also substitute the role of the conserved His residue in membrane anchor subunits. Although it has to be tested by protein chemically in future studies, our data support that the subunit structure of *Plasmodium* complex II is similar to that of mammalian complex II.

Properties of Plasmodium NDH-II—Previously, Krungkrai *et al.* (*47*) isolated mitochondrial complex I from *P. falciparum* and *P. berghei* as a 130-kDa complex containing 38- and 33-kDa subunits. They claimed that NADH:ubiquinone-8 reductase activity was sensitive to rotenone (IC_{50} = 12 μM) and plumbagin (IC_{50} = 6 μM). However, NDH-I is not encoded by the *Plasmodium* genomes (*6*, *7*) and concentrations of *n*-octyl glucoside used for the solubilization and purification were below its critical micelle concentration (CMC) where *n*-octyl glucoside cannot serve as a detergent. Alternative NADH dehydrogenase NDH-II is a rotenone-insensitive single-subunit enzyme (*15*, *34*) and the apparent molecular weights and subunit structure of *P. falciparum* (acc. no. XP_001352022 and MW 61,670) and *P. y. yoelii* (acc. no. XP_731423, MW 66,156) NDH-II are totally different from those reported by Krungkrai *et al.* (*47*). The IC_{50} value of mouse liver mitochondria for rotenone (8.4 μM; Table 3 in ref. 47) was three orders of magnitude higher than the IC_{50} reported for mammalian enzymes (*26*). Recently, Biagini *et al.* (*15*) used the whole cell lysate of *P. falciparum* and claimed that PfNDH-II was inhibited by diphenylene iodonium chloride (DPI, IC_{50} of 15–25 μM) and diphenyl iodonium chloride (IDP, IC_{50} = 66 μM). As pointed out by Vaidya *et al.* (*48*), the IC_{50} for the enzyme was 100- and 10-fold higher than those for the growth inhibition and other NADH oxidases in the lysate may contribute to the activity. Very recently, it was reported that purified recombinant PfNDH-II was not inhibited by known NDH-I inhibitors and flavoenzyme inhibitors (DPI and IDP) (Dong, C., Patel, V., Clardy, J., and Wirth, D., personal communication). Thus, previous studies on *Plasmodium* NDH-II need to be reexamined. Our data indicate that *Plasmodium* NDH-II is a member of internal NDH-II (Ndi), which reoxidizes NADH in the mitochondrial matrix. Recently, Saleh *et al.* (*49*) demonstrated the antiplasmodial activity (IC_{50} = 14 nM) of 1-hydroxy-2-dodecyl-4(1*H*)quinolone (HDQ), which has been identified as the potent inhibitor for *Y. lipolytica* NDE (IC_{50} = 0.2 μM) (*50*), demonstrating that *Plasmodium* NDH-II is a promising target for new drugs.

Oxidative Phosphorylation in Plasmodium Mitochondria—For a long time, it has been assumed that *Plasmodium* mitochondria cannot carry out oxidative phosphorylation (*4*, *5*) because of a lack of membrane anchor subunits of ATP synthase (*9*, *11*). Oxidative phosphorylation, succinate respiration (*8*, *17*), and effects of respiratory complex inhibitors on the generation of membrane potential (*16*) in rodent malaria mitochondria support the notion that *Plasmodium* mitochondria are fully capable of oxidative phosphorylation. Careful analysis of current genome databases (*6*, *7*) with partial subunits sequences of *Crithidia fasciculata* (*51*) and *Leishmania tarentolae* (*52*) could identify ten subunits of *P. falciparum* F_oF_1-ATP synthase, including membrane anchor subunits *a* (XP_001347344) and *b* (XP_001348969) (Mogi, T. and Kita, K., unpublished

results), which are found to be highly divergent from eukaryotic and bacterial counterparts. Thus, all canonical subunits of complex II and ATP synthase are present in *Plasmodium* spp., and malaria parasites can yield energy *via* oxidative phosphorylation. The *in vivo* expression profiles of parasites derived from infected patients showed the up-regulation of these enzymes under conditions similar to starvation in yeast (*18*).

CONCLUSION

We isolated active mitochondria from rodent malaria *P. y. yoelii* from infected mouse erythrocytes and characterized complex II and NDH-II. *Plasmodium* complex II is the four-subunit enzyme but its quinone-reduction site in the membrane anchor subunits seems structurally different from that of mammalian enzyme. *Plasmodium* NDH-II showed enzymatic properties similar to those of NDI and quinolones were found to be potent inhibitors. Alternative respiratory enzymes, which are absent in mammalian mitochondria, are as promising targets for new antibiotics (*53*, *54*). We hope that our findings will help understanding of energy metabolism in malaria parasites and the development of new antimalarial drugs.

FUNDING

This study was supported in part by a grant-in-aid for scientific research (20570124 to T.M.), scientific research on Priority Areas (18073004 to K.K.) and Creative Scientific Research (18GS0314 to K.K.) from the Japanese Ministry of Education, Science, Culture, Sports, and Technology. We thank Dr H. Ohtsuki (Ehime University) for *P. y. yoelii* strain 17XL, Dr. D. Wirth (Harvard School of Public Health) for the use of unpublished results prior to publication, and Ministry of Health, Labour and Welfare for financial supports.

CONFLICT OF INTEREST

None declared.

REFERENCES

1. World Health Organization (2007) Malaria Elimination. A field manual for low and moderate endemic countries. World Health Organization, Geneva, Switzerland
2. Hyde, J.E. (2005) Drug-resistant malaria. *Trends Parasitol.* **21**, 494–498
3. Sherman, I.W. (1998) Carbohydrate metabolism of asexual stages. in *Malaria, Parasite Biology, Pathogenesis and Protection* (Sherman, I.W., ed.), pp. 135–143, ASM Press, Washington, DC
4. Vaidya, A.B. (1998) Mitochondrial physiology as a target for atovaquone and other antimalarials. in *Malaria, Parasite Biology, Pathogenesis and Protection* (Sherman, I.W., ed.), pp. 355–368, ASM Press, Washington, DC
5. Van Dooren, G.G., Stimmler, L.M., and McFadden, G.I. (2006) Metabolic maps and functions of the *Plasmodium* mitochondrion. *FEMS Microbiol. Rev.* **30**, 596–630
6. Gardner, M.J., Hall, N., Fung, E., White, O., Berriman, M., Hyman, R.W., Carlton, J.M., Pain, A., Nelson, K.E., Bowman, S., Paulsen, I.T., James, K., Eisen, J.A., Rutherford, K., Salzberg, S.L., Craig, A., Kyes, S., Chan, M.S., Nene, V., Shallom, S.J., Suh, B., Peterson, J., Angiuoli, S., Pertea, M., Allen, J., Selengut, J., Haft, D., Mather, M.W., Vaidya, A.B., Martin, D.M., Fairlamb, A.H., Fraunholz, M.J., Roos, D.S., Ralph, S.A., McFadden, G.I., Cummings, L.M., Subramanian, G.M., Mungall, C., Venter, J.C., Carucci, D.J., Hoffman, S.L., Newbold, C., Davis, R.W., Fraser, C.M., and Barrell, B. (2002) Genome sequence of the human malaria parasite *Plasmodium falciparum*. *Nature* **419**, 498–511
7. Carlton, J.M., Angiuoli, S.V., Suh, B.B., Kooij, T.W., Pertea, M., Silva, J.C., Ermolaeva, M.D., Allen, J.E., Selengut, J.D., Koo, H.L., Peterson, J.D., Pop, M., Kosack, D.S., Shumway, M.F., Bidwell, S.L., Shallom, S.J., van Aken, S.E., Riedmuller, S.B., Feldblyum, T.V., Cho, J.K., Quackenbush, J., Sedegah, M., Shoaibi, A., Cummings, L.M., Florensk, L., Yatesk, J.R., Raine, J. D., Sinden, R.E., Harris, M.A., Cunningham, D.A., Preiser, P.R., Bergman, L.W., Vaidya, A.B., van Lin, L.H., Janse, C.J., Waters, A.P., Smith, H.O., White, O.R., Salzberg, S.L., Venter, J.C., Fraser, C.M., Hoffman, S.L., Gardner, M.J., and Carucci, D.J. (2002) Genome sequence and comparative analysis of the model rodent malaria parasite *Plasmodium yoelii yoelii*. *Nature* **419**, 512–519
8. Uyemura, S.A., Luo, S., Vieira, M., Moreno, S.N., and Docampo, R. (2004) Oxidative phosphorylation and rotenone-insensitive malate- and NADHquinone oxidoreductases in *Plasmodium yoelii yoelii* mitochondria *in situ*. *J. Biol. Chem.* **279**, 385–393
9. Matsushita, K., Ohnishi, T., and Kaback, H.R. (1987) NADH-ubiquinone oxidoreductases of the *Escherichia coli* aerobic respiratory chain. *Biochemistry* **26**, 7732–7737
10. Takeo, S., Kokaze, A., Ng, C.S., Mizuchi, D., Watanabe, J.I., Tanabe, K., Kojima, S., and Kita, K. (2000) Succinate dehydrogenase in *Plasmodium falciparum* mitochondria: molecular characterization of the *SDHA* and *SDHB* genes for the catalytic subunits, the flavoprotein (Fp) and iron–sulfur (Ip) subunits. *Mol. Biochem. Parasitol.* **107**, 191–205
11. Fry, M., Webb, E., and Pudney, M. (1990) Effect of mitochondrial inhibitors on adenosinetriphosphate levels in *Plasmodium falciparum*. *Comp. Biochem. Physiol. B* **96**, 775–782
12. Vaidya, A.B. and Mather, M.W.A. (2005) Post-genomic view of the mitochondrion in malaria parasites. *Curr. Top. Microbiol. Immunol.* **295**, 233–250
13. Painter, H.J., Morrisey, J.M., Mather, M.W., and Vaidya, A.B. (2007) Specific role of mitochondrial electron transport in blood-stage *Plasmodium falciparum*. *Nature* **446**, 88–91
14. Fry, M. and Pudney, M. (1992) Site of action of the antimalarial hydroxynaphthoquinone, 2-[trans-4-(4′-chlorophenyl)cyclohexyl]-3-hydroxy-1,4-naphthoquinone (566C80). *Biochem. Pharmacol.* **43**, 1545–1453
15. Biagini, G.A., Viriyavejakul, P., O'Neill, P.M., Bray, P.G., and Ward, S.A. (2006) Functional characterization and target validation of alternative Complex I of *Plasmodium falciparum* mitochondria. *Antimicrob. Agents Chemother.* **50**, 1841–1851
16. Srivastava, I.K., Rottenberg, H., and Vaidya, A.B. (1997) Atovaquone, a broad spectrum antiparasitic drug, collapses mitochondrial membrane potential in malarial parasite. *J. Biol. Chem.* **272**, 3961–3966
17. Uyemura, S.A., Luo, S., Moreno, S.N.J., and Docampo, R. (2000) Oxidative phosphorylation, Ca^{2+} transport, and fatty acid-induced uncoupling in malaria parasites mitochondria. *J. Biol. Chem.* **275**, 9709–9715
18. Daily, J.P., Scanfeld, D., Pochet, N., Roch, K.L., Plouffe, D., Kamel, M., Sarr, O., Mboup, S., Ndir, O., Wypij, D., Lavasseur, K., Thomas, E., Tamayo, P., Dong, C., Zhou, Y., Lander, E.S., Ndiaye, D., Wirth, D., Winzeler, E.A., Mesirov, J.P., and Regev, A. (2007)

Distinct physiological states of *Plasmodium falciparum* in malaria-infected patients. *Nature* **450**, 1091–1095
19. Homewood, C.A. and Neame, K.D. (1976) Comparison of methods used for removal of white cells from malaria-infected blood. *Ann. Trop. Med. Parasitol.* **70**, 249–251
20. Takashima, E., Takamiya, S., Takeo, S., Mi-ichi, F., Amino, H., and Kita, K. (2001) Isolation of mitochondria from *Plasmodium falciparum* showing dihydroorotate dependent respiration. *Parasitol. Int.* **50**, 273–278
21. Johnson, D. and Lardy, H. (1967) Isolation of liver or kidney mitochondria in *Methods Enzymol.* Vol. 10, (Estabrook, R.W. and Pullman, M.E., eds.), pp. 94–96, Academic Press, New York
22. Mogi, T., Ui, H., Shiomi, K., Ōmura, S., and Kita, K. (2008) Gramicidin S identified as a potent inhibitor for cytochrome *bd*-type quinol oxidase. *FEBS Lett.* **582**, 2299–2302
23. Wittig, I., Karas, M., and Schagger, H. (2007) High resolution clear native electrophoresis for in-gel functional assays and fluorescence studies of membrane protein complexes. *Mol. Cell Proteomics* **6**, 1215–1122
24. Kobayashi, T., Sato, S., Takamiya, S., Komaki-Yasuda, K., Yano, K., Hirata, A., Onitsuka, A., Hata, M., Mi-ichi, F., Tanaka, T., Hase, T., Miyajima, A., Kawazu, S., Watanabe, Y., and Kita, K. (2007) Mitochondria and apicoplast of *Plasmodium falciparum*: behaviour on subcellular fractionation and the implication. *Mitochondrion* **7**, 125–132
25. Mi-Ichi, F., Miyadera, H., Kobayashi, T., Takamiya, S., Waki, S., Iwata, S., Shibata, S., and Kita, K. (2005) Parasite mitochondria as a target of chemotherapy: inhibitory effect of licochalcone A on the *Plasmodium falciparum* respiratory chain. *Ann. NY Acad. Sci.* **1056**, 46–54
26. Ueno, H., Miyoshi, H., Ebisui, K., and Iwamura, H. (1994) Comparison of the inhibitory action of natural rotenone and its stereoisomers with various NADH-ubiquinone reductases. *Eur. J. Biochem.* **225**, 411–417
27. Tushurashvili, P.R., Gavrikova, E.V., Ledenev, A.N., and Vinogradov, A.D. (1985) Studies on the succinate dehydrogenating system. Isolation and properties of the mitochondrial succinate-ubiquinone reductase. *Biochim. Biophys. Acta* **809**, 145–159
28. Miyadera, H., Shiomi, K., Ui, H., Yamaguchi, Y., Masuma, R., Tomoda, H., Miyoshi, H., Osanai, A., Kita, K., and Omura, S. (2003) Atpenins, potent and specific inhibitors of mitochondrial complex II (succinate-ubiquinone oxidoreductase). *Proc. Natl Acad. Sci. USA* **100**, 473–477
29. Suraveratum, N., Krungkrai, S.R., Leangaramgul, P., Prapunwattana, P., and Krungkrai, J. (2000) Purification and characterization of *Plasmodium falciparum* succinate dehydrogenase. *Mol. Biochem. Parasitol.* **105**, 215–222
30. Yankovskaya, V., Horsefield, R., Tornroth, S., Luna-Chavez, C., Miyoshi, H., Leger, C., Byrne, B., Cecchini, G., and Iwata, S. (2003) Architecture of succinate dehydrogenase and reactive oxygen species generation. *Science* **299**, 700–704
31. Sun, F., Huo, X., Zhai, Y., Wang, A., Xu, J., Su, D., Bartlam, M., and Rao, Z. (2005) Crystal structure of mitochondrial respiratory membrane protein complex II. *Cell* **121**, 1043–1057
32. Huang, L.S., Sun, G., Cobessi, D., Wang, A.C., Shen, J.T., Tung, E.Y., Anderson, V.E., and Berry, E.A. (2006) 3-Nitropropionic acid is a suicide inhibitor of mitochondrial respiration that, upon oxidation by Complex II, forms a covalent adduct with a catalytic base arginine in the active site of the enzyme. *J. Biol. Chem.* **281**, 5965–5972
33. Schägger, H. and Pfeiffer, K. (2000) Supercomplexes in the respiratory chains of yeast and mammalian mitochondria. *EMBO J.* **19**, 1777–1783
34. Kerscher, S.J. (2000) Diversity and origin of alternative NADH:ubiquinone oxidoreductase. *Biochim. Biophys. Acta* **1459**, 274–283
35. De Vries, S. and Grivell, L.A. (1988) Purification and characterization of a rotenone-insensitive NADH:Q_6 oxidoreductase from mitochondria of *Saccharomyces cerevisiae*. *Eur. J. Biochem.* **176**, 377–341
36. Björklöf, K., Zickermann, V., and Finel, M. (2000) Purifiction of the 45 kDa, membrane bound NADH dehydrogenase of *Escherichia coli* (NDH-2) and analysis of its interaction with ubiquinone analogs. *FEBS Lett.* **467**, 105–110
37. Kerscher, S.J., Okun, J.G., and Brandt, U. (1999) A single external enzyme confers alternative NADH:ubiquinone oxidoreductase activity in *Yarrowia lipolytica*. *J. Cell Sci.* **112**, 2347–2354
38. Rasmusson, A.G., Fredlund, K.M., and Møller, I.M. (1993) Purification of a rotenone-insensitive NAD(P)H dehydrogenase from the inner surface of red beetroot mitochondria. *Biochim. Biophys. Acta* **1141**, 107–110
39. Luethy, M.H., Thelen, J.J., Knudten, A.F., and Elthon, T.E. (1995) Purification, characterization, and submitochondrial localization of a 58-kilodalton NAD(P)H dehydrogenase. *Plant Physiol.* **107**, 443–450
40. Yamashita, T., Nakamaru-Ogiso, E., Miyoshi, H., Matsuo-Yagi, A., and Yagi, T. (2007) Roles of bound quinone in the single subunit NADH-quinone oxidoreductase (Ndi1) from *Saccharomyces cerevisiae*. *J. Biol. Chem.* **282**, 6012–6020
41. Miyoshi, H., Takegami, K., Sakamoto, K., Mogi, T., and Iwamura, H. (1999) Characterization of the ubiquinol oxidation sites in cytochromes *bo* and *bd* from *Escherichia coli* using aurachin C analogues. *J. Biochem.* **125**, 138–142
42. Yano, T., Li, L.-S., Weinstein, E., The, J.-S., and Rubin, H. (2006) Steady-state kinetics and inhibitory action of antitubercular phenothiazines on *Mycobacterium tuberculosis* type-II NADH-menaquinone oxidoreductase (NDH-2). *J. Biol. Chem.* **281**, 11456–11463
43. Roos, M.H. and Tielens, A.G.M. (1994) Differential expression of two succinate dehydrogenase subunit-B genes and a transition in energy metabolism during the development of the parasitic nematode *Haemonchus contortus*. *Mol. Biochem. Parasitol.* **66**, 273–281
44. Saruta, F., Kuramochi, T., Nakamura, K., Takamiya, S., Yu, Y., Aoki, T., Sekimizu, K., Kojima, S., and Kita, K. (1995) Stage-specific isoforms of complex II (succinate-ubiquinone oxidoreductase) in mitochondria from the parasitic nematode, *Ascaris suum*. *J. Biol. Chem.* **270**, 928–932
45. Morales, J., Mogi, T., and Kita, K. (2008) Divergence in structure of mitochondrial respiratory Complex II (succinate-ubiquinone reductase) revealed by protozoan enzymes. *Biochim. Biophys. Acta* **1777**, S94–S95
46. Oyedotun, K.S. and Lemire, B.D. (1999) The *Saccharomyces cerevisiae* succinate-ubiquinone oxidoreductase. Identification of Sdh3p amino acid residues involved in ubiquinone binding. *J. Biol. Chem.* **274**, 23956–23962
47. Krungkrai, J., Kanchanarithisak, R., Krungkrai, S.R., and Sunant Rochanakij, S. (2002) Mitochondrial NADH dehydrogenase from *Plasmodium falciparum* and *Plasmodium berghei*. *Exp. Parasitol.* **100**, 54–61
48. Vaidya, A.B., Painter, H.J., Morrisey, J.M., and Mather, M.W. (2008) The validity of mitochondrial dehydrogenases as antimalarial drug targets. *Trends Parasitol.* **24**, 8–9
49. Saleh, A., Friesen, J., Baumeister, S., Gross, G., and Bohne, W. (2007) Growth inhibition of *Toxoplasma gondii* and *Plasmodium falciparum* by nanomolar concentrations of 1-hydroxy-2-dodecyl-4(1*H*)quinolone, a high-affinity inhibitor of alternative (type II) NADH dehydrogenases. *Antimicrob. Agents Chemother.* **51**, 1217–1222
50. Eschemann, A., Galkin, A., Oettmeier, W., Brandt, U., and Kerscher, S. (2005) HDQ (1-hydroxy-2-dodecyl-4(1*H*)quinolone), a high affinity inhibitor for mitochondrial

alternative NADH dehydrogenase: evidence for a ping-pong mechanism. *J. Biol. Chem.* **280**, 3138–3142

51. Speijer, D., Breek, C.K., Muijsers, A.O., Hartog, A.F., Berden, J.A., Albracht, S.P., Samyn, B., van Beeumen, J., and Benne, R. (1997) Characterization of the respiratory chain from cultured *Crithidia fasciculate*. *Mol. Biochem. Parasitol.* **85**, 171–186
52. Nelson, R.E., Aphasizheva, I., Falick, A.M., Nebohacova, M., and Simpson, L. (2004) The I-complex in *Leishmania tarentolae* is an uniquely-structured F_1-ATPase. *Mol. Biochem. Parasitol.* **135**, 221–224
53. Minagawa, N., Yabu, Y., Kita, K., Nagai, K., Ohta, N., Meguro, K., Sakajo, S., and Yoshimoto, A. (1997) An antibiotic, ascofuranone, specifically inhibits respiration and in vitro growth of long slender bloodstream forms of *Trypanosoma brucei brucei*. *Mol. Biochem. Parasitol* **84**, 271–280
54. Saimoto, H., Shigemasa, Y., Kita, K., Yabu, Y., Hosokawa, T., and Yamamoto, M. (2007) Novel phenol derivatives and antitrypanosoma preventive/therapeutic agent comprising the same as active ingredient. U.S. Patent 20070208078

Biochimica et Biophysica Acta 1787 (2009) 129–133

Contents lists available at ScienceDirect

Biochimica et Biophysica Acta

journal homepage: www.elsevier.com/locate/bbabio

Antibiotics LL-Z1272 identified as novel inhibitors discriminating bacterial and mitochondrial quinol oxidases

Tatsushi Mogi [a,*], Hideaki Ui [b], Kazuro Shiomi [b], Satoshi Ōmura [b], Hideto Miyoshi [c], Kiyoshi Kita [a]

[a] Department of Biomedical Chemistry, Graduate School of Medicine, The University of Tokyo, Hongo, Bunkyo-ku, Tokyo 113-0033, Japan
[b] Kitasato Institute for Life Sciences and Graduate School of Infection Control Sciences, Kitasato University, Shirokane, Minato-ku, Tokyo 108-8641, Japan
[c] Division of Applied Life Sciences, Graduate School of Agriculture, Kyoto University, Sakyo-ku, Kyoto 606-8502, Japan

ARTICLE INFO

Article history:
Received 9 October 2008
Received in revised form 21 November 2008
Accepted 26 November 2008
Available online 10 December 2008

Keywords:
Quinol oxidase
Inhibitor
Natural antibiotic
Escherichia coli
Trypanosoma brucei
Alternative oxidase

ABSTRACT

To counter antibiotic-resistant bacteria, we screened the Kitasato Institute for Life Sciences Chemical Library with bacterial quinol oxidase, which does not exist in the mitochondrial respiratory chain. We identified five prenylphenols, LL-Z1272β, γ, δ, ε and ζ, as new inhibitors for the *Escherichia coli* cytochrome *bd*. We found that these compounds also inhibited the *E. coli bo*-type ubiquinol oxidase and trypanosome alternative oxidase, although these three oxidases are structurally unrelated. LL-Z1272β and ε (dechlorinated derivatives) were more active against cytochrome *bd* while LL-Z1272γ, δ, and ζ (chlorinated derivatives) were potent inhibitors of cytochrome *bo* and trypanosome alternative oxidase. Thus prenylphenols are useful for the selective inhibition of quinol oxidases and for understanding the molecular mechanisms of respiratory quinol oxidases as a probe for the quinol oxidation site. Since quinol oxidases are absent from mammalian mitochondria, LL-Z1272β and δ, which are less toxic to human cells, could be used as lead compounds for development of novel chemotherapeutic agents against pathogenic bacteria and African trypanosomiasis.

1. Introduction

The emergence of antibiotic-resistant strains of major pathogenic bacteria such as *Staphylococcus aureus* is an increasingly serious public health concern [1]. To evade bacterial drug-resistance mechanisms, new effective chemotherapeutic agents, which have novel mechanisms of action as well as different cellular targets compared with conventional antibiotics, need to be developed [2].

Cytochromes *bo* (CyoABCD) and *bd* (CydAB) are two terminal quinol oxidases of the aerobic respiratory chain in *Escherichia coli* and many other bacteria [3,4 for reviews]. Although they are structurally unrelated, both generate proton-motive force through the oxidation of quinols coupled to dioxygen reduction. Cytochrome *bo* is a proton-pumping heme–copper terminal oxidases and is predominantly expressed under highly aerated growth conditions. In contrast, cytochrome *bd* is a predominant terminal oxidase under microaerophilic growth conditions and performs a variety of physiological functions such as microaerophilic respiration and protection against oxygen stress. Further, cytochrome *bd* and its variant cyanide-insensitive oxidase (CioAB) play a key role in survival and adaptation of pathogenic bacteria that encounter host environments where dioxygen is progressively limited [5–9].

In long slender bloodstream forms of the parasitic protist *Trypanosoma brucei*, which causes sleeping sickness in human and nagana in livestock, mitochondrial respiratory Complexes III and IV are down-regulated and alternative quinol oxidase (AOX) serves as a terminal oxidase [10,11]. AOX is a di-iron family protein bound to the matrix side of the inner membrane and cannot generate the proton-motive force. All three quinol oxidases have no counterparts in mammalian mitochondria, thus they are potential targets for novel antimicrobial chemotherapeutics. In fact, we previously identified ascofuranone (AF), a prenylphenol isolated from a phytopathogenic fungus *Ascochyta viciae* [12], as a potent inhibitor for the growth of *T. brucei* and trypanosome AOX (noncompetitive inhibition with IC_{50} of 2 nM) [13,14].

By screening of hundreds of natural antibiotics in the Kitasato Institute for Life Sciences Chemical Library [15] with the *E. coli* cytochrome *bd*, we found that LL-Z1272γ has potent inhibititory activity. We extended our screening to related compounds and found that antibiotics LL-Z1272β, γ, δ, ε and ζ (Fig. 1), prenylphenols isolated from the fungus *Verticillum* sp. FO-2787 [16], are a unique set of natural compounds that can discriminate and inhibit alternative respiratory quinol oxidases. Thus, antibiotics LL-Z1272 are useful probes for understanding of molecular mechanisms of quinol oxidases and we hope that our findings contribute to the development of new antibiotics.

2. Materials and methods

2.1. Isolation or source of antibiotics and inhibitors

LL-Z1272β, γ, δ, ε and ζ were isolated from the cultured mycelium *Verticillum* sp. FO-2787 [16]. Antibiotics LL-Z1272α, β, γ,

* Corresponding author. Tel.: +81 3 5841 8202; fax: +81 3 5841 3444.
E-mail address: tmogi@m.u-tokyo.ac.jp (T. Mogi).

0005-2728/$ – see front matter © 2008 Elsevier B.V. All rights reserved.
doi:10.1016/j.bbabio.2008.11.016

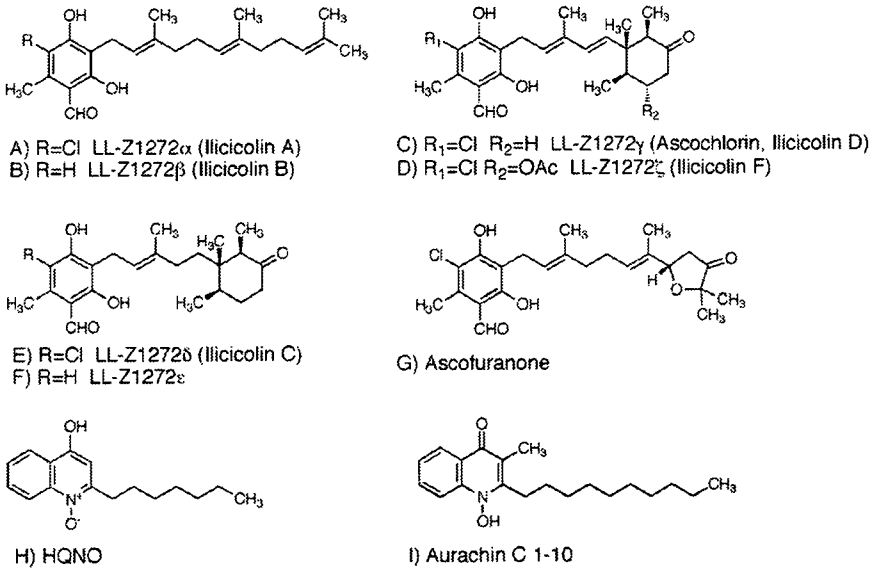

Fig. 1. Structures of antibiotics LL-Z1272 and related natural compounds.

δ, ε and ζ have been originally isolated from an imperfect fungus *Fusarium* sp. as inhibitors for the growth of the protist *Tetrahymena pyriformis* [17]. Ilicicolin A, B, D, C, and F isolated from the fungus *Cylindrocladium ilicicola* [18] are also identical to LL-Z1272α, β, γ, δ, and ζ, respectively [19]. AF and piericidin A were kind gifts from Drs. Masaichi Yamamoto (aRigen Pharmaceuticals. Inc.) and Shigeo Yoshida (Institute of Physical and Chemical Research), respectively. Synthesis of aurachin C 1-10 was described previously [20]. Antimycin A_1 and 2-heptyl-4-hydroxyquinoline *N*-oxide (HQNO) were purchased from Sigma.

2.2. Preparation of cytoplasmic membrane vesicles and purification of cytochrome bo

Cytochrome *bd*-overproduced membranes were isolated from *E. coli* ST4683/pNG2 (Δ*cyo* Δ*cyd*/*cyd*$^+$ Tet^R), which can overproduce *bd*-type quinol oxidase as the sole terminal oxidase [21]. Heme *d* content was 2.1±0.1 nmol/mg protein (*i.e.* approximately 20% of membrane proteins). Cytochrome *bo*-type quinol oxidase was purified from cytoplasmic membranes of *E. coli* GO103/pHN3795-1 (*cyo*$^+$ Δ*cyd*/*cyo*$^+$ Amp^R), as described previously [22]. Trypanosome AOX-overproduced membranes were isolated from *E. coli* FN102 (BL21 (DE3) Δ*hemA*)/pTvAOX, which can express *Trypanosoma vivax* AOX as the sole functional quinol oxidase [23]. The expression level of AOX was estimated to be ~5% of membrane proteins by SDS-polyacrylamide gel electrophoresis.

2.3. Quinol oxidase assay

The activity of the *E. coli* quinol oxidases was determined at 25 °C with a V-660 double monochromatic spectrophotometer (JASCO, Tokyo, Japan) with data acquisition at 0.05 s. The reaction mixture (1 ml) contained 50 mM potassium phosphate (pH 6.5), and 0.02% Tween 20 (protein grade, Calbiochem) [24]. Enzyme concentrations were 2.4 nM for cytochrome *bd* and 2 nM for cytochrome *bo*. Reactions were started by addition of ubiquinol-1 (Q_1H_2) at a final concentration of 100 μM, and the activity was calculated by using a molar extinction coefficient of 12,300 at 278 nm. The activity of *T. vivax* AOX was measured in 50 mM Tris–HCl (pH 7.4)–0.1% sucrose monolaurate (Mitsubishi-Kagaku Foods Co., Tokyo, Japan). Enzyme kinetics were analyzed based on the modified *ping-pong bi-bi* mechanism for cytochrome *bd* [21] or the Michaelis–Menten mechanism for cytochrome *bo* and *T. vivax* AOX, by using KaleidaGraph ver. 4.0 (Synergy Software, Reading, PA).

2.4. Dose-response analysis

Duplicate assays were performed at each concentration with two independent preparations of membranes. Dose–response data were analyzed by the nonlinear regression curve-fitting with KaleidaGraph ver. 4.0 as described previously [24]. IC_{50} values in the presence of 100 μM Q_1H_2 were estimated by using the equation for the relative residual activity; $v=1/(1+([\text{Inhibitor}]/IC_{50})^n)$ where n is the Hill coefficient [24].

3. Results

3.1. Analysis of inhibition of cytochrome bd by antibiotics LL-Z1272

In the course of our screening for inhibitors against the *E. coli* cytochrome *bd*, we identified LL-Z1272γ as an antibiotic that suppressed the Q_1H_2 oxidation by the cytochrome *bd*-overproduced membranes (84% inhibition at 5 μg/ml) greater than antimycin A (50%), a non-competitive inhibitor of cytochrome *bd* [25]. We extended our screening with antibiotics LL-Z1272β, γ, δ, ε and ζ, prenylphenols isolated from *Verticillum* sp. FO-2787 [16], and found that LL-Z1272β and ε were more potent inhibitors for cytochrome *bd*. These compounds do not have a chlorine atom at position 5 of the phenol ring (Fig. 1), and the cyclohexanone ring of LL-Z1272ε slightly increased the binding affinity to cytochrome *bd* (Table 1). The 50% inhibitory concentrations (IC_{50}) for LL-Z1272β and ε (dechlorinated derivatives) were determined to be 2.1 and 1.1 μM (average values of two independent preparations), respectively, and are one-order of magnitude smaller than those of LL-Z1272γ, δ and ζ (chlorinated derivatives) (Table 1). The IC_{50} values for known inhibitors for cytochrome *bd* [20,25–27] are 10 μM for piericidin A, 5 μM for antimycin A, 1 μM for HQNO, and 8.3 nM for aurachin C 1–10.

Table 1
Summary on IC_{50} values of quinol oxidase inhibitors for the *E. coli* cytochrome *bd* and *bo* and *T. vivax* AOX

Compounds	Cytochrome *bd*[a]	Cytochrome *bo*[b]	trypanosome AOX[c]
LL-Z1272β	2.1±0.1[d]	1.2±0.1	0.18±0.02
LL-Z1272γ	81±17	0.082±0.016	0.015±0.001
LL-Z1272δ	32±4	0.28±0.02	0.046±0.004
LL-Z1272ε	1.1±0.1	7.2±0.7	0.65±0.09
LL-Z1272ζ	85±7	0.37±0.02	0.43±0.02
Ascofuranone	47±10	0.062±0.003	0.0049±0.0002
Aurachin C 1–10	0.0083±0.0003	0.0023±0.0001	28±2

[a] The *E. coli* cytochrome *bd*-overproduced membranes.
[b] The purified *E. coli* cytochrome *bo*.
[c] The *T. vivax* AOX-overproduced membranes.
[d] μM.

3.2. Kinetic analysis of inhibition of cytochrome bd by LL-Z1272β and ε

Effects of LL-Z1272β and ε on the Q_1H_2 oxidation by cytochrome *bd* were further analyzed kinetically. Control data were analyzed based on the modified *ping-pong bi-bi* mechanism by assuming the stabilization of dioxygen reduction intermediates [28] and apparent K_m and V_{max} values for the control were determined to 50 μM and 2364 Q_1H_2/enzyme/s, respectively, in 50 mM potassium phosphate (pH 6.5)–0.02% Tween 20 [24] (Fig. 2). In the presence of inhibitors, reactions followed the Michaelis–Menten kinetics (Fig. 2). LL-Z1272β acts as a noncompetitive inhibitor with K_i=7.6±2.5 μM while LL-Z1272ε serves as a competitive inhibitor with K_i=1.00±0.03 μM (Fig. 2).

3.3. Dose–response analysis of inhibition of cytochrome bo by antibiotics LL-Z1272

In contrast to *bd*-type oxidase, the Q_1H_2 oxidase activity of the *E. coli* cytochrome *bo* was more sensitive to chlorinated derivatives, LL-Z1272γ, ε and ζ. IC_{50} values for LL-Z1272β, γ, δ, ε and ζ (averages from two preparations) were determined to be 1.2, 0.082, 0.28, 7.2 and 0.37 μM, respectively (Table 1). The IC_{50} values for known inhibitors for cytochrome *bo* [20,27,29–31] are 0.3 μM for HQNO, 0.14 μM for piericidin A, and 2.3 nM for aurachin C 1–10, showing that cytochrome *bo* is more sensitive to these quinone analogs than cytochrome *bd*. It should be noted that LL-Z1272γ is a very potent inhibitor of cytochrome *bo*.

3.4. Kinetic analysis of inhibition of cytochrome bo by antibiotics LL-Z1272

Effects of LL-Z1272β, γ, δ, and ζ on the Q_1H_2 oxidation by cytochrome *bo* were further analyzed kinetically at different concentrations of inhibitors. Enzyme kinetics were analyzed based on the Michaelis–Menten mechanism [29,31], and we found that the inhibition mechanism was all mixed-type (Fig. 3). It should be noted that due to changes in assay conditions apparent K_m and V_{max} values were shifted to 23 μM and 1035 Q_1H_2/enzyme/s, respectively (Fig. 3), from 50 μM and 515 Q_1H_2/enzyme/s, respectively, in 50 mM Tris–HCl (pH 7.4)–0.1% sucrose monolaurate in our previous study [32].

3.5. Dose–response analysis of inhibition of trypanosome AOX by antibiotics LL-Z1272

Because of the structural similarity of antibiotics LL-Z1272 with trypanocidal AF (Fig. 1), we examined the effects of antibiotics LL-Z1272 on Q_1H_2 oxidase activity of *T. vivax* AOX. From dose–response analysis with the AOX-overproduced *E. coli* membranes, we determined IC_{50} values for LL-Z1272β, γ, δ, ε, ζ, AF and aurachin C1–10 to be 180, 15, 46, 650, 430, 4.9 nM and 28 μM, respectively (Table 1). Our data indicate that 1) the furanone ring of AF is not essential for binding to trypanosome AOX, 2) the 5-chloride group on the phenol ring increases the binding affinity, and 3) aurachin C, the most potent inhibitor for bacterial quinol oxidases (IC_{50}=8.3 and 2.3 nM for the *E. coli* cytochrome *bd* and *bo*, respectively (Table 1)) [20,27], is 2 to 4 order of magnitude less active than the prenylphenols.

3.6. Kinetic analysis of inhibition of trypanosome AOX by antibiotics LL-Z1272

Effects of LL-Z1272β, γ, δ, ε and ζ and AF on enzyme kinetics by *T. vivax* AOX were examined in the presence of detergents. Q_1H_2 oxidation by *T. vivax* AOX followed the Michaelis–Menten kinetics

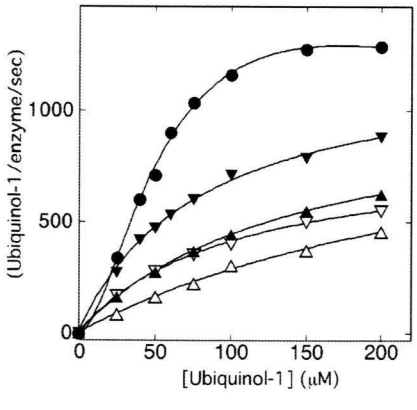

Fig. 2. Effects of antibiotics LL-Z1272 on kinetic parameters for Q_1H_2 oxidation by the *E. coli* cytochrome *bd*. Kinetic analysis was carried out in the absence of inhibitors (●) and the presence of 2 (▼) or 5 (▽) μM LL-Z1272β or 2 (▲) or 5 (△) μM LL-Z1272ε. Control data was analyzed by using the equation $v=SV_{max}/(SS(1+S/K_S)+SK_m+K_mK_m)$ where K_S indicates the constant for substrate inhibition. Data obtained in the presence of inhibitors were analyzed based on the Michaelis–Menten kinetics. The apparent K_m (μM) and V_{max} (Q_1H_2/enzyme) values obtained were 50±4 and 2364±194, respectively, for the control (K_S=381 μM), 79±5 and 1232±33, respectively, for 2 μM LL-Z1272β, 100±5 and 826±21, respectively, for 5 μM LL-Z1272β, 140±3 and 1065±12, respectively, for 2 μM LL-Z1272ε, 287±41 and 1113±107 Q_1H_2/enzyme/s, respectively, for 5 μM LL-Z1272ε, respectively.

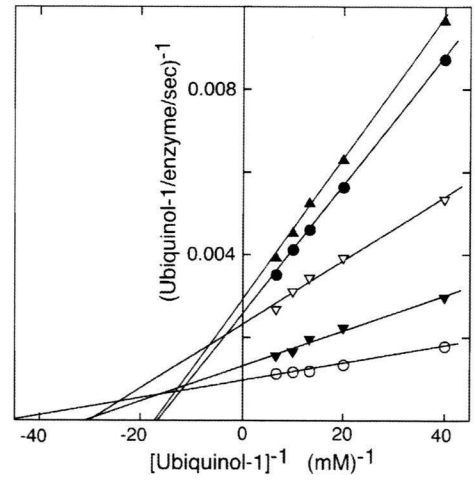

Fig. 3. Effects of antibiotics LL-Z1272 on kinetic parameters for Q_1H_2 oxidation by the *E. coli* cytochrome *bo*. Kinetic analysis was carried out in the absence of inhibitors (○) and the presence of 0.75 μM LL-Z1272β (▼), 0.2 μM LL-Z1272γ (●), 0.75 μM LL-Z1272δ (▲), and ζ (▽). Data were analyzed based on the Michaelis–Menten kinetics. The apparent K_m and V_{max} values obtained are 23±2 and 1035±28 (control), 43±4 and 841±30 (0.75 μM LL-Z1272β), 64±2 and 402±4 (0.2 μM LL-Z1272γ), 66±3 and 361±6 (0.75 μM LL-Z1272δ), 46±4 μM and 486±14 Q_1H_2/enzyme/s (0.75 μM LL-Z1272ζ), respectively. *R* values were >0.997.

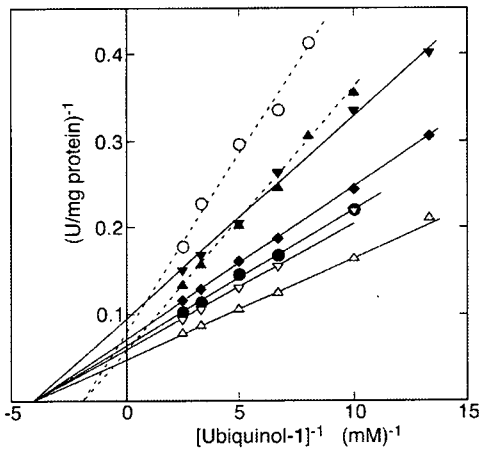

Fig. 4. Effects of antibiotics LL-Z1272 on kinetic parameters for Q_1H_2 oxidation by trypanosome AOX. Kinetic analysis was carried out in the absence of inhibitors (△) and the presence of 200 nM LL-Z1272β (▼), 20 nM LL-Z1272γ (●), 50 nM LL-Z1272δ (▲), 1 μM LL-Z1272ε (○) and 50 nM LL-Z1272ζ (▽), and 5 nM AF (◆). For clarity we showed data for one concentration of each inhibitor. The apparent K_m and V_{max} values determined for the control were 232 μM and 19.8 U/mg protein, respectively. The apparent K_i values for non-competitive inhibition by LL-Z1272β, γ, ζ, and AF were 142, 59, 203, and 2.65 nM. K_i and K_i' values for mixed-type inhibition by LL-Z1272δ and LL-Z1272ε were 0.032 and 25.5 μM and 0.483 and 9.61 μM, respectively.

and apparent K_m and V_{max} values were determined to be 232 μM and 20 U/mg protein (Fig. 4). The K_m value in 0.1% sucrose monolaurate was comparable to 350 μM for *T. b. brucei* AOX in 0.25% *n*-octyl-β-D-glucopyranoside *plus* 0.025% EDT-20 [34], but smaller than approximately 700 μM determined for *T. b. brucei* AOX in the absence of detergents [13,23]. Since the K_m value of *T. vivax* AOX for ubiquinol-2 was 116 μM (data not shown), the length of the isoprene unit may increase the binding affinity for ubiquinones [35]. The K_m of trypanosome AOX for ubiquinol-9 in *T. b. brucei* mitochondria would be comparable to the K_m value of cytochrome *bd* for ubiquinol-8 in *E. coli*.

Kinetic analysis of inhibition of *T. vivax* AOX by antibiotics LL-Z1272 revealed that LL-Z1272β (K_i=142 nM), γ (59 nM), and ζ (203 nM) act as (apparently) non-competitive inhibitors (Fig. 4), as reported for AF [13] and salicylhydroxamic acid (SHAM, K_i=25 μM) [34]. Since the amount of active AOX molecules in the *E. coli* membranes was difficult to estimate, we did not try kinetic analysis for tight-binding inhibitors [36]. In contrast, LL-Z1272δ and ε serve as mixed-type inhibitors with K_i and K_i' values of 0.032 and 25.5 μM and 0.483 and 9.61 μM, respectively.

4. Discussion

From the screening of natural antibiotics of the Kitasato Institute for Life Sciences Chemical Library, we identified prenylphenols LL-Z1272β, γ, δ, ε and ζ as a unique set of inhibitors, which can inhibit and discriminate bacterial and trypanosomal ubiquinol oxidases (Table 1). LL-Z1272β and ε (dechlorinated derivatives) inhibited cytochrome *bd*-type oxidase while LL-Z1272γ, δ, and ζ (chlorinated derivatives) were potent inhibitors of cytochrome *bo*-type oxidase and trypanosome AOX. Aurachin C is a potent inhibitor for both cytochrome *bo* and *bd* [20,27], while AF is more active against trypanosome AOX [13]. Since all three quinol oxidases are absent from mammalian mitochondria, prenylphenols could be used as lead compounds for development of novel chemotherapeutic agents [13,14,37]. However, except for the effect of LL-Z1272β on *Clostridium perfringens* (minimum inhibitory concentration of 25 μg/ml), antibiotics LL-Z1272 were ineffective against *S. aureus*, *Pseudomonas aeruginosa*, *Mycobacterium smegmatis*, and *Bacteroides fragilis*. Neither LL-Z1272γ nor LL-Z1272ε affected the aerobic growth of *E. coli* cells expressing cytochrome *bo* or *bd* as the sole terminal oxidase, likely due to the excretion by drug efflux pumps or due to the inefficient penetration through the lipopolysaccharide layer of the outer membrane.

Kinetic analysis of the inhibition of quinol oxidases by prenylphenols yielded rather complicated inhibition mechanisms (Figs. 2–4). Structural similarities of prenylphenols to ubiquinones (Fig. 1) indicate that all these compounds would act as competitive inhibitors for the quinol oxidation site. However, in many cases we found non-competitive or mixed type inhibition. In the case of tight binding inhibitors [36], Michaelis–Menten plots resemble to those of non-competitive inhibition. Alternatively, orientation of the phenol ring of prenylphenol molecules within the binding pocket will determine interactions of prenyl tails and/or the cyclohexanone ring with the protein moiety. The latter interactions would affect the former interactions. In addition, modifications of the prenyl tail (*i.e.*, the presence of the cyclohexanone or franone ring) could alter interactions with lipid bilayers and detergent micelles, which would then affect the orientation of inhibitor molecules relative to the binding pocket in quinol oxidases. Inhibition mechanisms of natural antibiotics may be inherently associated with their structural complexity, as found for inhibitors for alternative NADH dehydrogenase NDH-II [38].

Currently approved drugs for the treatment of human sleeping sickness caused by *T. b. rhodesiense* and *T. b. gambiense* are suramine, pentamidine, melarsoprol, and eflornithine [37]. They are not available for oral administration and *T. brucei* strains resistant to one or more drugs are now emerging. Thus there is an urgent need for less-toxic and more convenient new drugs against African trypanosomiasis. In parallel studies, we recently found trypanocidal activity of LL-Z1272β [39]. LL-Z1272β and LL-Z1272δ have been shown to be less toxic to human cells [18,33] and we have demonstrated that the efficacy of AF in the treatment of trypanosome-infected mice [14]. In conclusion, antibiotics LL-Z1272 are useful as probes for understanding the quinol oxidation sites of respiratory quinol oxidases and such prenylphenols are promising leading compounds for the development of new chemotherapeutic agents for African trypanosomiasis.

Acknowledgements

We thank Dr. M. Yamamoto (aRigen Pharmaceuticals. Inc., Tokyo) for AF, Dr. S. Yoshida (Institute of Physical and Chemical Research, Saitama) for piericidin A, Dr. Rokuro Masuma (Kitasato Institute for Life Sciences) for measurements of antibacterial activities of antibiotics LL-Z1272, Dr. K. Matsushita (Yamaguchi University) for his advice on enzyme assay and Dr. R. B. Gennis (University of Illinois) for the plasmid pNG2 and the *E. coli* strain GO103. This study was supported by a Grant-in-Aid for Scientific Research (20570124 to TM), Scientific Research on Priority Areas (18073004 to KK) and Creative Scientific Research (18GS0314 to KK) from the Japanese Ministry of Education, Science, Culture, Sports, and Technology.

References

[1] T.J. Foster, The *Staphylococcus aureus* "superbug", J. Clin. Invest. 114 (2004) 1693–1696.
[2] J. Travis, Reviving the antibiotic miracle? Science 264 (1994) 360–362.
[3] S. Jünneman, Cytochrome *bd* terminal oxidase, Biochim. Biophys. Acta 1321 (1997) 107–127.
[4] T. Mogi, M. Tsubaki, H. Hori, H. Miyoshi, H. Nakamura, Y. Anraku, Two terminal quinol oxidase families in *Escherichia coli*: variations on molecular machinery for dioxygen reduction, J. Biochem. Mol. Biol. Biophys. 2 (1998) 79–110.
[5] L. Cunningham, M. Pitt, H.D. Williams, The *cioAB* genes from *Pseudomonas aeruginosa* code for a novel cyanide-insensitive terminal oxidase related to the cytochrome *bd* quinol oxidases, Mol. Microbiol. 24 (1997) 579–591.
[6] S.S. Way, S. Sallustio, R.S. Magliozzo, M.B. Goldberg, Impact of either elevated or decreased levels of cytochrome *bd* expression on *Shigella flexneri* virulence, J. Bacteriol. 181 (1999) 1229–1237.

[7] S. Endley, D. McMurray, T.A. Ficht, Interruption of the *cydB* locus in *Brucella abortus* attenuates intracellular survival and virulence in the mouse model of infection, J. Bacteriol. 183 (2001) 2454–2462.
[8] A.K. Turner, L.Z. Barber, P. Wigley, S. Muhammad, M.A. Jones, M.A. Lovell, S. Hulme, P.A. Barrow, Contribution of proton-translocating proteins to the virulence of *Salmonella enterica* serovars Typhimurium, Gallinarum, and Dublin in chickens and mice, Infect. Immun. 71 (2003) 3392–3401.
[9] L. Shi, C.D. Sohaskey, B.D. Kana, S. Dawes, R.J. North, V. Mizrahi, M.L. Gennaro, Changes in energy metabolism of *Mycobacterium tuberculosis* in mouse lung and under *in vitro* conditions affecting aerobic respiration, Proc. Natl. Acad. Sci. U. S. A. 102 (2005) 15629–15634.
[10] M. Chaudhuri, R.D. Ott, G.C. Hill, Trypanosome alternative oxidase: from molecule to function, Trends Parasitol. 22 (2006) 484–491.
[11] A.L. Moore, M.S. Albury, P.G. Crichton, C. Affourtit, Function of the alternative oxidase: is it still a scavenger? Trends Plant Sci. 7 (2002) 478–481.
[12] N. Sasaki, T. Okutomi, T. Hosokawa, Y. Nawata, K. Ando, Ascofuranone, a new antibiotic from *Ascochyta viciae*, Tetrahedron Lett. 13 (1972) 2541–2544.
[13] N. Minagawa, Y. Yabu, K. Kita, K. Nagai, N. Ohta, K. Meguro, S. Sakajo, A. Yoshimoto, An antibiotic, ascofuranone, specifically inhibits respiration and in vitro growth of long slender bloodstream forms of *Trypanosoma brucei brucei*. Mol, Biochem. Parasitol. 84 (1997) 271–280.
[14] Y. Yabu, A. Yoshida, T. Suzuki, C. Nihei, K. Kawai, N. Minagawa, T. Hosokawa, K. Nagai, K. Kita, N. Ohta, The efficacy of ascofuranone in a consecutive treatment on *Trypanosoma brucei brucei* in mice, Parasitol. Int. 52 (2003) 155–164.
[15] H. Ui, A. Ishiyama, H. Sekiguchi, M. Namatame, A. Nishihara, A. Takahashi, K. Shiomi, K. Otoguro, S. Ō mura, Selective and potent *in vitro* antimalarial activities found in four microbial metabolites, J. Antibiot. 60 (2007) 220–222.
[16] S. Takamatsu, M.-C. Rho, R. Masuma, M. Hayashi, K. Komiyama, H. Tanaka, S. Omura, A novel testosterone 5a-reductase inhibitor, 8′9′-dehydroascochlorin produced by *Verticillium* sp. FO-2787, Chem. Pharm. Bull. 42 (1994) 953–956.
[17] G.A. Ellestad, R.H. Evans Jr., M.P. Kunstmann, Terpenoid metabolites from an unidentified *Fusarium* species, Tetrahedron 25 (1969) 1323–1334.
[18] S. Hayakawa, H. Minato, K. Katagiri, The ilicicolins, antibiotics from *Cylindrocladium ilicicola*, J. Antibiot. 24 (1971) 653–654.
[19] H. Minato, T. Katayama, S. Hayakawa, K. Katagiri, Identification of ilicicolins with ascochlorin and LL-Z1272, J. Antibiot. 25 (1972) 315–316.
[20] H. Miyoshi, K. Takegami, K. Sakamoto, T. Mogi, H. Iwamura, Characterization of the ubiquinol oxidation sites in cytochromes *bo* and *bd* from *Escherichia coli* using aurachin C analogues, J. Biochem. 125 (1999) 138–142.
[21] T. Mogi, S. Endo, S. Akimoto, M. Morimoto-Tadokoro, H. Miyoshi, Glutamates 99 and 107 in transmembrane helix III of subunit I of cytochrome *bd* are critical for binding of the heme b_{595}-*d* binuclear center and enzyme activity, Biochemistry 45 (2006) 15785–15792.
[22] M. Tsubaki, T. Mogi, Y. Anraku, H. Hori, Structure of heme–copper binuclear center of the cytochrome *bo* complex of *Escherichia coli*: EPR and Fourier-transform infrared spectroscopic studies, Biochemistry 32 (1993) 6065–6072.
[23] T. Suzuki, C. Nihei, Y. Yabu, T. Hashimoto, M. Suzuki, A. Yoshida, K. Nagai, T. Hosokawa, N. Minagawa, S. Suzuki, K. Kita, N. Ohta, Molecular cloning andcharacterization of *Trypanosoma vivax* alternative oxidase (AOX) gene, a target of the trypanocide ascofuranone, Parasitol. Int. 53 (2004) 235–245.
[24] T. Mogi, H. Ui, K. Shiomi, S. Ōmura, K. Kita, Gramicidin S identified as a potent inhibitor for cytochrome *bd*-type quinol oxidase, FEBS Lett. 582 (2008) 2299–2302.
[25] S. Jünemann, J.M. Wrigglesworth, Antimycin inhibition of the cytochrome *bd* complex from *Azotobacter vinelandii* indicates the presence of a branched electron transfer pathway for the oxidation of ubiquinol, FEBS Lett. 345 (1994) 198–202.
[26] K. Kita, K. Konishi, Y. Anraku, Terminal oxidases of *Escherichia coli* aerobic respiratory chain. II. Purification and properties of cytochrome b_{558}-*d* complex from cells grown with limited oxygen and evidence of branched electron-carrying systems, J. Biol. Chem. 259 (1984) 3375–3381.
[27] B. Meunier, S.A. Madgwick, E. Reil, W. Ottemeier, P.R. Rich, New inhibitors of the quinol oxidation sites of bacterial cytochromes *bo* and *bd*, Biochemistry 34 (1995) 1076–1083.
[28] Y. Matsumoto, E. Muneyuki, D. Fujita, K. Sakamoto, H. Miyoshi, M. Yoshida, T. Mogi, Kinetic mechanism of quinol oxidation by cytochrome *bd* studied with ubiquinone-2 analogs, J. Biochem. 139 (2006) 779–788.
[29] K. Kita, K. Konishi, Y. Anraku, Terminal oxidases of *Escherichia coli* aerobic respiratory chain. I. Purification and properties of cytochrome b_{562}-*o* complex from cells in the early exponential phase of aerobic growth, J. Biol. Chem. 259 (1984) 3368–3374.
[30] K. Matsushita, L. Patel, H.R. Kaback, Cytochrome *o* oxidase from *Escherichia coli*. Characterization of the enzyme and mechanism of electrochemical proton gradient generation, Biochemistry 23 (1984) 4703–4714.
[31] M. Sato-Watanabe, T. Mogi, H. Miyoshi, H. Iwamura, K. Matsushita, O. Adachi, Y. Anraku, Structure–function studies on the ubiquinol oxidation site of the cytochrome *bo* complex from *Escherichia coli* using *p*-benzoquinones and substituted phenols, J. Biol. Chem. 269 (1994) 28899–28907.
[32] T. Mogi, T. Hirano, H. Nakamura, Y. Anraku, Y. Orii, Cu_B promotes both binding and reduction of dioxygen at the heme–copper binuclear center in the *Escherichia coli bo*-type ubiquinol oxidase, FEBS Lett. 370 (1995) 259–263.
[33] M. Gutiérrez, C. Theoduloz, J. Rodríguez, M. Lolas, G. Schmeda-Hirschmann, Bioactive metabolites from the fungus *Nectria galligena*, the main apple canker agent in Chile, J. Agric. Food Chem. 53 (2005) 7701–7708.
[34] R. Ott, K. Chibale, S. Anderson, A. Chipeleme, M. Chaudhuri, A. Guerrah, N. Colowick, G.C. Hill, Novel inhibitors of the trypanosome alternative oxidase inhibit *Trypanosoma brucei brucei* growth and respiration, Acta Trop. 100 (2006) 172–184.
[35] K. Sakamoto, H. Miyoshi, M. Ohshima, K. Kuwabara, K. Kano, T. Akagi, T. Mogi, H. Iwamura, Role of isoprenyl tail of ubiquinone in reaction with respiratory enzymes: studies with bovine heart mitochondrial complex I and *Escherichia coli bo*-type ubiquinol oxidase, Biochemistry 37 (1998) 15106–15113.
[36] P.R. Rich, S.A. Madgwick, D.A. Moss, The interactions of duroquinol, DBMIB and NQNO with the chloroplast cytochrome *bf* complex, Biochim. Biophys. Acta 1058 (1991) 312–328.
[37] A.H. Fairlamb, Chemotherapy of human African trypanosomiasis: current and future prospect, Trends Parasitol. 19 (2003) 488–494.
[38] T. Mogi, K. Matsushita, H. Miyoshi, H. Ui, K. Shiomi, S. Ômura, K. Kita, Identification of new inhibitors for alternative NADH dehydrogenase (NDH-II). FEMS Microbiol. Lett. (in press).
[39] K. Otoguro, A. Ishiyama, M. Namatame, A. Nishihara, T. Furusawa, R. Masuma, K. Shiomi, Y. Takahashi, H. Yamada, S. Omura, Selective and potent *in vitro* antitrypanosomal activities of ten microbial metabolites, J. Antibiot. 61 (2008) 372–378.

Glossary

AOX: alternatice quinol oxidase
HQNO: 2-heptyl-4-hydroxyquinoline *N*-oxide
IC_{50}: IC_{50}, the 50% inhibitory concentration
Q_1H_2: a reduced form of Q_1, ubiquinol-1

Cell Metabolism
Article

Fasting-Induced Hypothermia and Reduced Energy Production in Mice Lacking Acetyl-CoA Synthetase 2

Iori Sakakibara,[1,2] Takahiro Fujino,[3] Makoto Ishii,[2,4] Toshiya Tanaka,[1] Tatsuo Shimosawa,[5] Shinji Miura,[6] Wei Zhang,[7] Yuka Tokutake,[8] Joji Yamamoto,[2,9] Mutsumi Awano,[10] Satoshi Iwasaki,[1,2] Toshiyuki Motoike,[2,11] Masashi Okamura,[1,9] Takeshi Inagaki,[1] Kiyoshi Kita,[10] Osamu Ezaki,[6] Makoto Naito,[13] Tomoyuki Kuwaki,[7] Shigeru Chohnan,[8] Tokuo T. Yamamoto,[14] Robert E. Hammer,[12] Tatsuhiko Kodama,[1] Masashi Yanagisawa,[2,11] and Juro Sakai[1,2,*]
[1]Laboratory for Systems Biology and Medicine, Research Center for Advanced Science and Technology, University of Tokyo, Tokyo 153-8904, Japan
[2]ERATO, Japan Science and Technology Agency (JST), Tokyo 102-0075, Japan
[3]Department of Bioscience, Integrated Center for Sciences, Ehime University Graduate School of Medicine, Ehime 791-0295, Japan
[4]Department of Neurology, Weill Cornell Medical College of Cornell University, 525 East 68th Street, New York, NY 10021, USA
[5]Department of Clinical Laboratory, Faculty of Medicine, University of Tokyo, Tokyo 113-8655, Japan
[6]Nutritional Science Program, National Institute of Health and Nutrition, 1-23-1, Toyama, Shinjuku-ku, Tokyo 162-8636, Japan
[7]Departments of Molecular & Integrative Physiology and Autonomic Physiology, Graduate School of Medicine, Chiba University, Chiba, 260-8670, Japan
[8]Department of Bioresource Science, Ibaraki University College of Agriculture, 3-21-1 Chuo, Ami, Ibaraki 300-0393, Japan
[9]Division of Nephrology, Endocrinology, and Vascular Medicine, Department of Medicine, Tohoku University Graduate School of Medicine, Sendai 980-8574, Japan
[10]Department of Biomedical Chemistry, Graduate School of Medicine, University of Tokyo, Bunkyo-ku, Tokyo 113-0033, Japan
[11]Howard Hughes Medical Institute, Department of Molecular Genetics
[12]Department of Biochemistry
University of Texas Southwestern Medical Center, Dallas, TX 75390, USA
[13]Department of Cellular Function, Division of Cellular and Molecular Pathology, Niigata University Graduate School of Medical and Dental Sciences, Niigata 951-8510, Japan
[14]Center for Advanced Genome Research, Institute of Development, Aging, and Cancer, Tohoku University, Sendai 981-8555, Japan
*Correspondence: jmsakai-tky@umin.ac.jp
DOI 10.1016/j.cmet.2008.12.008

SUMMARY

Acetate is activated to acetyl-CoA by acetyl-CoA synthetase 2 (AceCS2), a mitochondrial enzyme. Here, we report that the activation of acetate by AceCS2 has a specific and unique role in thermogenesis during fasting. In the skeletal muscle of fasted *AceCS2*$^{-/-}$ mice, ATP levels were reduced by 50% compared to *AceCS2*$^{+/+}$ mice. Fasted *AceCS2*$^{-/-}$ mice were significantly hypothermic and had reduced exercise capacity. Furthermore, when fed a low-carbohydrate diet, 4-week-old weaned *AceCS2*$^{-/-}$ mice also exhibited hypothermia accompanied by sustained hypoglycemia that led to a 50% mortality. Therefore, AceCS2 plays a significant role in acetate oxidation needed to generate ATP and heat. Furthermore, *AceCS2*$^{-/-}$ mice exhibited increased oxygen consumption and reduced weight gain on a low-carbohydrate diet. Our findings demonstrate that activation of acetate by AceCS2 plays a pivotal role in thermogenesis, especially under low-glucose or ketogenic conditions, and is crucially required for survival.

INTRODUCTION

Mammals have evolved complex metabolic systems to survive extended periods of nutrient deprivation. Under a fed condition, mammals utilize glucose as the main metabolic fuel. Under ketogenic conditions such as fasting, low-carbohydrate diet feeding, and diabetes, fatty acids and ketone bodies are utilized as the main energy sources. Ketone bodies, utilized mainly in brain and also some in skeletal muscle and heart (Fukao et al., 2004), are produced in liver from acetyl-CoA released after β oxidation of fatty acids in mitochondria. Several lines of evidence report that acetate is synthesized in the liver and utilized as an alternative fuel under ketogenic conditions. For instance, acetate concentration in livers of starved rats is quite high (Murthy and Steiner, 1973). Also, formation of free acetate by the liver has been reported from studies utilizing isolated rat liver perfusion and studies using isolated hepatocytes (Leighton et al., 1989; Seufert et al., 1974; Yamashita et al., 2001). Acetate is generated following hydrolysis of acetyl-CoA by acetyl CoA hydrolase, an end product of fatty acid oxidation in rat liver peroxisomes (Leighton et al., 1989). However, it is not known whether acetate is actually utilized as an alternative fuel (substituting for glucose, fatty acids, or ketone bodies) in peripheral tissues such as skeletal muscle, heart, brown adipose tissues (BAT), or brain.

Acetyl-CoA synthetase (AceCS, EC 6.2.1.1) ligates acetate and CoA to generate acetyl-CoA. In mammals, there are two AceCSs with similar enzymatic properties: one, designated AceCS1, is a cytosolic enzyme, whereas AceCS2 is an enzyme of the mitochondrial matrix (Fujino et al., 2001; Luong et al., 2000). AceCS1 and AceCS2 are regulated posttranscriptionally by members of the sirtuin family of deacetylases, SIRT1 and SIRT3, respectively. Both SIRT1 and SIRT3 are upregulated during caloric restriction and have been implicated as mediating

the longevity-promoting effects of caloric restriction (Schwer and Verdin, 2008; Yang et al., 2007).

AceCS1 provides acetyl-CoA for the synthesis of fatty acids and cholesterol. AceCS1 is highly expressed in liver, and its transcription is regulated by sterol regulatory element-binding proteins (SREBPs), basic helix-loop-helix leucine zipper transcription factors that activate multiple genes involved in cholesterol and fatty acid metabolism (Ikeda et al., 2001; Luong et al., 2000). By contrast, AceCS2 produces acetyl-CoA for oxidation through the tricarboxylic acid cycle to produce ATP and CO_2 (Fujino et al., 2001). AceCS2 is highly expressed in BAT, heart, and skeletal muscle. Importantly, the levels of its mRNAs in BAT, heart, and skeletal muscle are robustly increased under ketogenic conditions, whereas the level of its mRNAs in liver was barely detectable (Fujino et al., 2001). The fasting-induced transcriptional activation of AceCS2 in the skeletal muscle is largely controlled by Krüppel-like factor 15 (KLF15), a member of the Krüppel-like family of transcription factors (Yamamoto et al., 2004) that regulates many genes involved in gluconeogenesis such as phosphoenolpyruvate carboxykinase (PEPCK) and amino acid-degrading enzymes required under ketogenic conditions (Gray et al., 2007; Teshigawara et al., 2005).

To examine whether acetate is utilized as a fuel under ketogenic conditions, we generated *AceCS2*-deficient mice. In this paper, we show that AceCS2 is essential for energy expenditure under ketogenic conditions.

RESULTS

Generation of *AceCS2*-Deficient Mice

To evaluate the role of AceCS2 in vivo, we generated mice lacking *AceCS2*. We constructed an insertion-type vector that disrupts exon 1 of the mouse *AceCS2* gene (Figure 1A). Two lines of mice harboring insertions in *AceCS2* were identified by Southern blotting (Figure 1B). Genotyping was performed by PCR (Figure 1C), and the absence of AceCS2 transcripts (Figure 1D) and protein (Figure 1E) was confirmed by quantitative real-time PCR (QRT-PCR) and immunoblot analysis, respectively. Wild-type (*AceCS2*$^{+/+}$), heterozygous (*AceCS2*$^{+/-}$), and homozygous (*AceCS2*$^{-/-}$) mice were born at frequencies predicted by simple Mendelian ratios. *AceCS2*$^{-/-}$ mice of both sexes were normally fertile and typical in appearance. No histological abnormalities were seen following light microscopy of sections obtained from multiple tissues of adult male mice, including bone, brain, stomach, heart, intestine, kidney, liver, pancreas, white adipose tissue, BAT, and skeletal muscle (data not shown). At birth, the body weight and length of *AceCS2*$^{-/-}$ mice were indistinguishable from their littermates. By the time of weaning (4 weeks of age), both male and female *AceCS2*$^{-/-}$ mice exhibited significant growth retardation (Figures S1A–S1C available online). After weaning, *AceCS2*$^{-/-}$ mice fed on normal chow diet began to catch up with *AceCS2*$^{+/+}$ mice in both body weight and body length. By 20 weeks of age, the body weight of the *AceCS2*$^{-/-}$ mice became comparable to their littermates (Figures S1A and S1B). Food intake of 4-week-old *AceCS2*$^{-/-}$ mice was slightly decreased compared to *AceCS2*$^{+/+}$ mice but became comparable to that of their littermates by 20 weeks of age (Figure S1D). Plasma parameters of *AceCS2*$^{+/+}$ and *AceCS2*$^{-/-}$ mice before weaning (2–4 weeks of age) and at 26 weeks of age are shown in Table S1. Glucose, ketone bodies, nonesterified fatty acids (NEFA), and insulin levels were indistinguishable between *AceCS2*$^{+/+}$ and *AceCS2*$^{-/-}$ mice at both 2–4 weeks of age and at 26 weeks of age (Table S1). Plasma concentration of growth hormone and

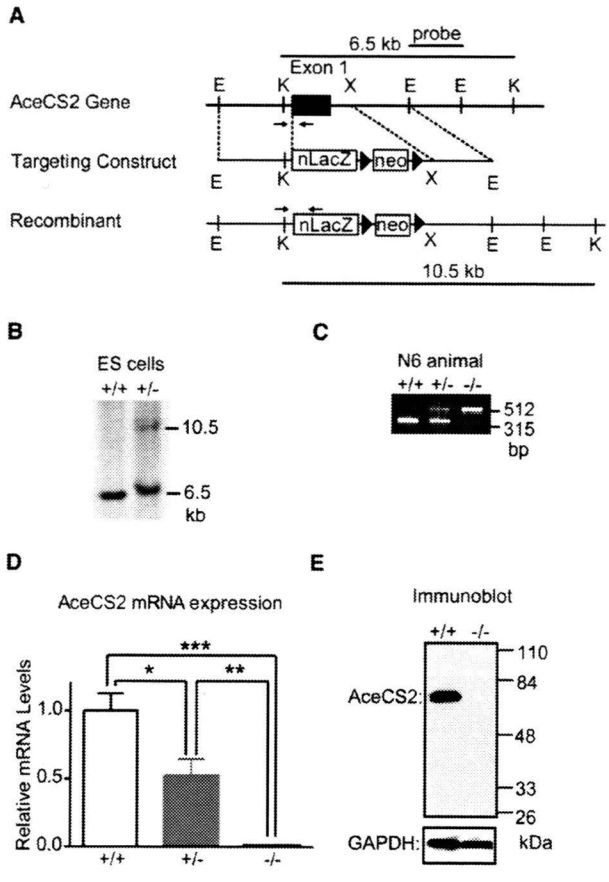

Figure 1. Generation of *AceCS2*-Deficient Mice

(A) Diagram of the targeting strategy. Only the relevant restriction sites are indicated. Locations of the probes for Southern blot analysis (bars) and PCR primers (arrows) for genotyping are shown.

(B) Southern blot analysis of KpnI-digested DNA from ES cell clones. Southern blotting was performed with the probe indicated in (A). KpnI digestion resulted in a 6.5 kb fragment in wild-type DNA and a 10.5 kb fragment in homologous recombinants.

(C) An ethidium bromide-stained agarose gel illustrates PCR products for genotyping *AceCS2*$^{+/+}$, *AceCS2*$^{+/-}$, and *AceCS2*$^{-/-}$ mice. A description of the PCR genotyping strategy is contained in the Experimental Procedures.

(D) QRT-PCR analysis of AceCS2 transcripts. Total RNA from heart of *AceCS2*$^{+/+}$, *AceCS2*$^{+/-}$, and *AceCS2*$^{-/-}$ mice were analyzed by QRT-PCR quantification as described in the Experimental Procedures. β-actin was used as the invariant control. Values represent the amount of mRNA relative to that in *AceCS2*$^{+/+}$ mice, which is arbitrarily defined as 1. Data are mean ± SEM. *$p < 0.05$ compared to *AceCS2*$^{+/+}$; **$p < 0.01$ compared to *AceCS2*$^{+/-}$; ***$p < 0.001$ compared to *AceCS2*$^{+/+}$ ($^{+/+}$, n = 9; $^{+/-}$, n = 17; $^{-/-}$, n = 7).

(E) Immunoblot analysis, with an affinity-purified anti-rabbit polyclonal AceCS2 antibody, of *AceCS2*$^{+/+}$ and *AceCS2*$^{-/-}$ mouse heart protein. Each lane was loaded with 20 μg of whole-cell lysates in SDS lysis buffer from the hearts. GAPDH was detected with a polyclonal anti-GAPDH antibody as a loading control.

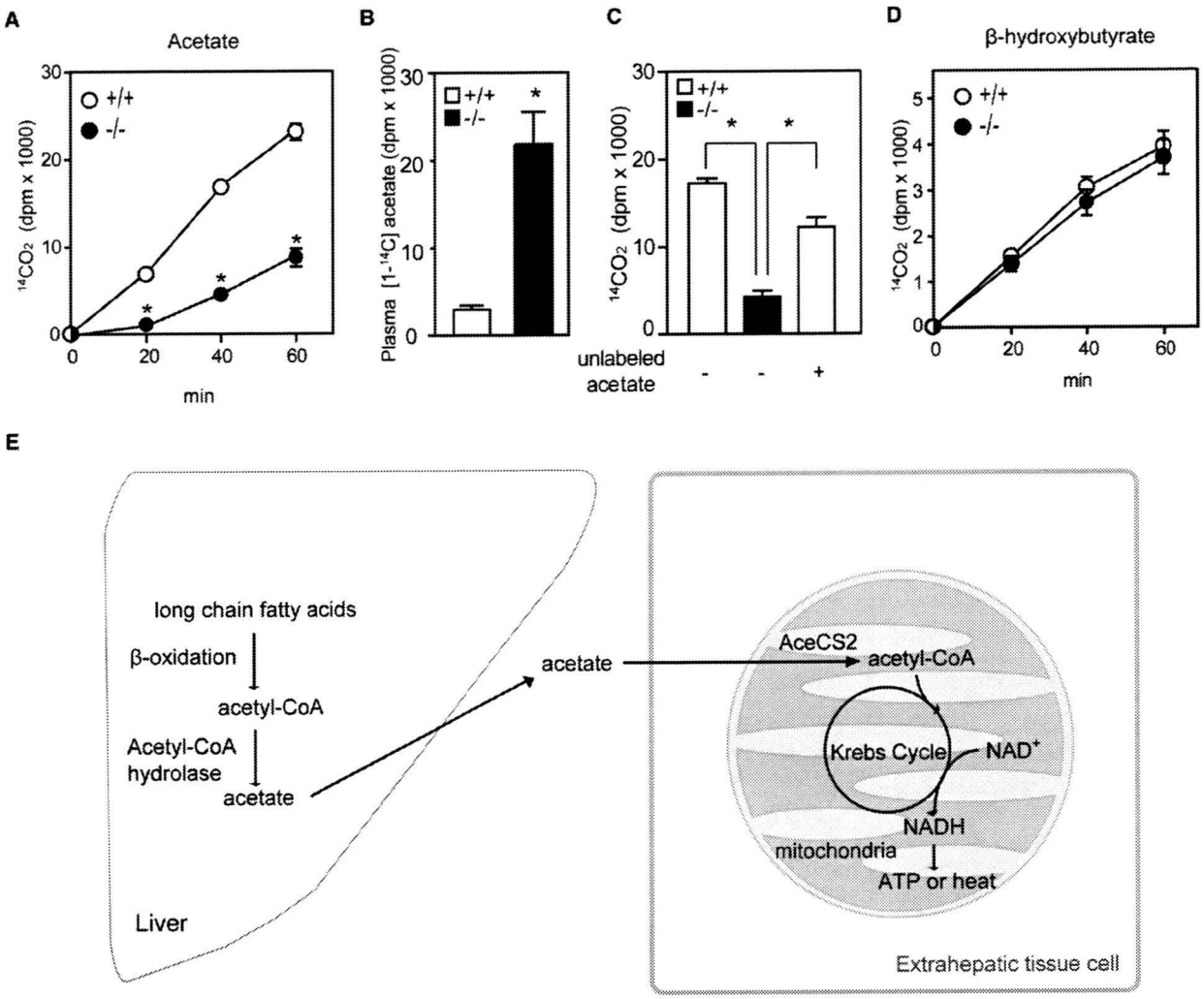

Figure 2. *AceCS2*$^{-/-}$ Mice Exhibit Lower Whole-Body Acetic Acid Oxidation during Fasting

After 48 hr of fasting, 12-week-old male mice were tested for their ability to oxidize [1-^{14}C]acetate or [1-^{14}C]β-hydroxybutyrate to $^{14}CO_2$ at 20, 40, and 60 min after intraperitoneal (i.p.) injection with the labeled compound.

(A) Rate of $^{14}CO_2$ production from acetate. *$p < 0.001$ compared to *AceCS2*$^{+/+}$.

(B) Total plasma [1-^{14}C]acetate was measured after 60 min.

(C) Rate of $^{14}CO_2$ production from acetate with inclusion of unlabeled acetate. Unlabeled acetate (0.6 g/kg) was injected with [1-^{14}C]acetate, and the acetate oxidation rate was measured after 40 min.

(D) Rate of $^{14}CO_2$ production from β-hydroxybutyrate (*AceCS2*$^{+/+}$, n = 6; *AceCS2*$^{-/-}$, n = 6).

(E) Model for the role of AceCS2 in energy metabolism.

(A–D) Data are mean ± SEM.

insulin-like growth factor-1 (IGF-1) of *AceCS2*$^{-/-}$ mice (2–4 weeks of age) were also comparable to *AceCS2*$^{+/+}$. The plasma leptin levels of 2- to 4-week-old *AceCS2*$^{-/-}$ mice were lower than those of age-matched, wild-type littermates. Notably, plasma acetate levels were markedly elevated in *AceCS2*$^{-/-}$ mice compared to *AceCS2*$^{+/+}$ mice (Table S1).

AceCS2$^{-/-}$ Mice Exhibited Marked Reduction in Whole-Body Acetate Oxidation

To examine whether acetate is, in fact, utilized as a fuel during fasting, we performed whole-body acetate oxidization assays. Mice were fasted for 48 hr and then injected with [^{14}C]acetate. Figure 2A shows the sharply decreased rate of acetate oxidation in *AceCS2*$^{-/-}$ mice. As a consequence, [^{14}C]acetate levels remained high in the plasma of *AceCS2*$^{-/-}$ mice, whereas *AceCS2*$^{+/+}$ mice showed very low levels of plasma [^{14}C]acetate (Figure 2B). Because higher levels of plasma acetate in *AceCS2*$^{-/-}$ mice might affect the acetate oxidation rate, we also examined the oxidation of [^{14}C]acetate with the inclusion of unlabeled acetate at similar levels to those found in the *AceCS2*$^{-/-}$ mice (about 2 mM) (Figure 2C). Injection of unlabeled acetate (0.6 mg/kg) led to rapid increase in plasma acetate to

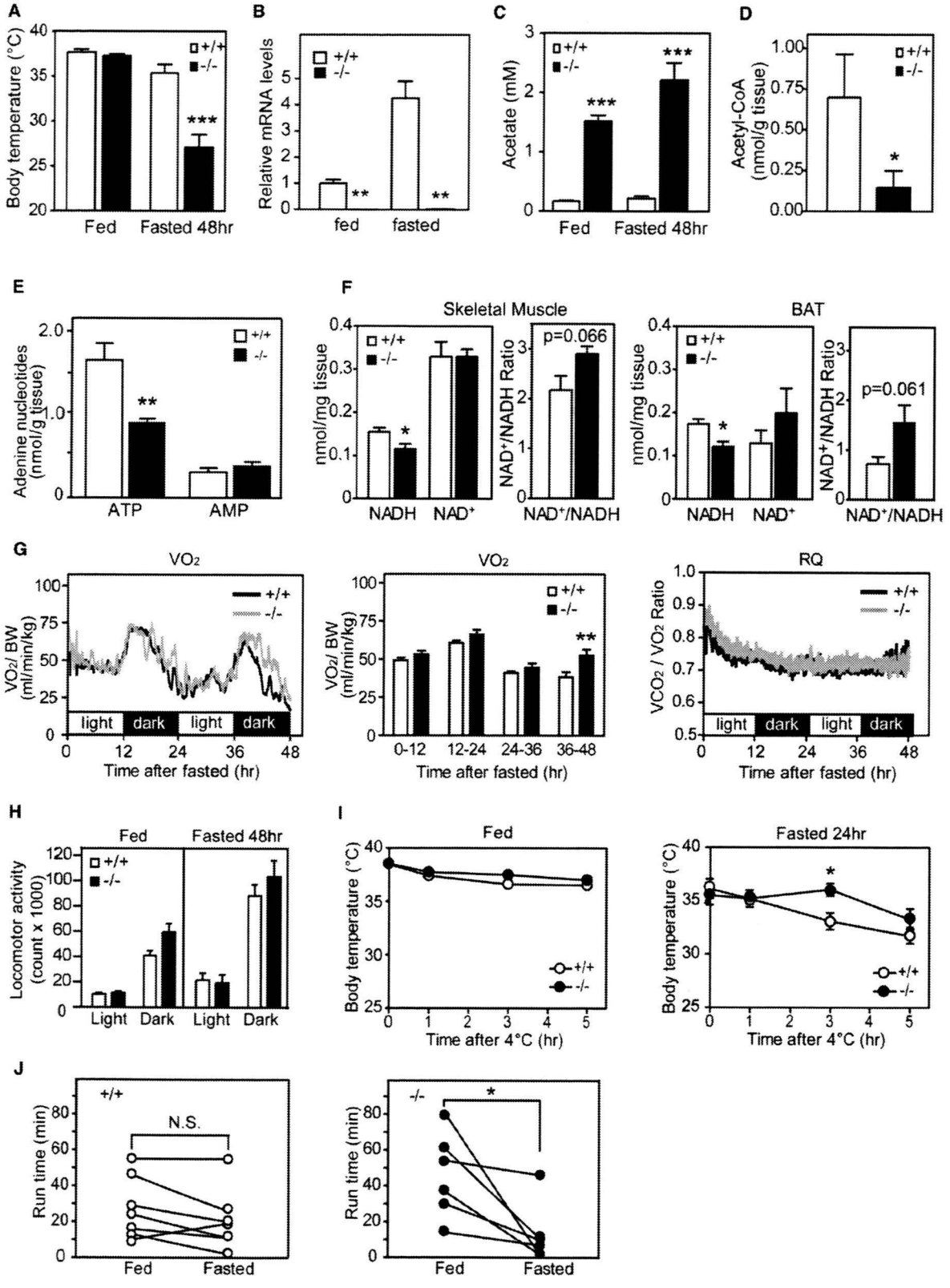
A
Body temperature (°C)
40
35
30
25
20
+/+
-/-
***
Fed
Fasted 48hr
B
Relative mRNA levels
5
4
3
2
1
0
+/+
-/-
**
**
fed
fasted
C
Acetate (mM)
3
2
1
0
+/+
-/-
***
***
Fed
Fasted 48hr
D
Acetyl-CoA (nmol/g tissue)
1.00
0.75
0.50
0.25
0.00
+/+
-/-
*
E
Adenine nucleotides (nmol/g tissue)
2.0
1.0
0
+/+
-/-
**
ATP
AMP
F
Skeletal Muscle
nmol/mg tissue
0.4
0.3
0.2
0.1
0
+/+
-/-
*
NADH
NAD+
NAD+/NADH Ratio
3
2
1
0
p=0.066
NAD+/NADH
BAT
nmol/mg tissue
0.4
0.3
0.2
0.1
0
+/+
-/-
*
NADH
NAD+
NAD+/NADH Ratio
3
2
1
0
p=0.061
NAD+/NADH
G
VO2
VO2/ BW (ml/min/kg)
100
75
50
25
0
+/+
-/-
light
dark
light
dark
0
12
24
36
48
Time after fasted (hr)
VO2
VO2/ BW (ml/min/kg)
100
75
50
25
0
+/+
-/-
**
0-12
12-24
24-36
36-48
Time after fasted (hr)
RQ
VCO2 / VO2 Ratio
1.0
0.9
0.8
0.7
0.6
0.5
+/+
-/-
light
dark
light
dark
0
12
24
36
48
Time after fasted (hr)
H
Fed
Fasted 48hr
Locomotor activity (count x 1000)
120
100
80
60
40
20
0
+/+
-/-
Light
Dark
Light
Dark
I
Fed
Body temperature (°C)
40
35
30
25
+/+
-/-
0
1
2
3
4
5
Time after 4°C (hr)
Fasted 24hr
Body temperature (°C)
40
35
30
25
*
+/+
-/-
0
1
2
3
4
5
Time after 4°C (hr)
J
+/+
N.S.
Run time (min)
80
60
40
20
0
Fed
Fasted
-/-
*
Run time (min)
80
60
40
20
0
Fed
Fasted

2 mM at 40 min after the injection (data not shown). Under this condition, the rate of acetate oxidation measured was still significantly lower in *AceCS2*$^{-/-}$ mice (Figure 2C). Oxidation of ketone bodies was similar, irrespective of genotype (Figure 2D), indicating that ketone body utilization is normal in *AceCS2*$^{-/-}$ mice.

Together with our previous report showing that [^{14}C]acetate is incorporated into CO_2 in AceCS2-transfected cells (Fujino et al., 2001), these data indicate that, in mice, acetate oxidation to form CO_2 and ATP requires AceCS2. Previous studies showed that an appreciable amount of acetate is generated in liver by hepatic acetyl-CoA hydrolase, a ubiquitous peroxisome enzyme, and that this acetate can subsequently be utilized by extrahepatic tissues (Leighton et al., 1989; Murthy and Steiner, 1973; Seufert et al., 1974). We propose a model in which acetate is generated in liver from fatty acids and released into the circulation under conditions when glucose is low, such as 48 hr fasting or low-carbohydrate/ high-fat diet. AceCS2 is necessary for salvaging this acetate for use in extrahepatic tissues such as skeletal muscle and BAT, where acetate is reactivated for reentry to the mitochondrial TCA cycle to generate ATP and heat (Figure 2E).

Adult *AceCS2*$^{-/-}$ Mice Exhibit Low Body Temperature and Reduced Capacity to Sustain Running Exercise under a Fasting Condition

To further evaluate the physiological role of acetate oxidation, 12-week-old *AceCS2*$^{-/-}$ mice were freely fed a standard rodent diet or fasted for 48 hr. During normal fed states, there was no significant difference in core temperature between *AceCS2*$^{+/+}$ and *AceCS2*$^{-/-}$ mice (Figure 3A). After 48 hr of fasting, *AceCS2*$^{+/+}$ mice were able to maintain their core body temperatures, but *AceCS2*$^{-/-}$ mice had significantly lower core body temperatures (Figure 3A). These data demonstrate that acetate activation by AceCS2 is important for maintenance of normal body temperature, likely as a result of heat production during fasting. Indeed, the mRNA levels in BAT of AceCS2 were 4-fold higher under the fasted condition than under the fed condition, suggesting that AceCS2 has an important role during fasting condition (Figure 3B).

In mice, BAT and skeletal muscle are the main thermogenic tissues in which oxidation of fatty acid, stimulated by the sympathetic nervous system, generates heat through uncoupling proteins (UCPs) present in mitochondria (Spiegelman and Flier, 2001). During fasting, the quantity and morphology of mitochondria in BAT and skeletal muscle are indistinguishable between *AceCS2*$^{+/+}$ mice and sex- and age-matched *AceCS2*$^{-/-}$ mice (Figure S2A). Oxidative proteins such as UCPs are thought to be important in thermogenesis (Matthias et al., 2000; Spiegelman and Flier, 2001). The mRNA levels of UCP1 in the BAT or UCP2 and UCP3 in the skeletal muscle did not differ significantly between *AceCS2*$^{+/+}$ and *AceCS2*$^{-/-}$ mice. Other thermogenic molecules PGC1α and PPARδ also did not differ in mRNA levels (Figure S2B and data not shown).

To evaluate substrate supply, we determined the levels of various metabolites in the plasma of fed and 48 hr fasted 12-week-old male *AceCS2*$^{+/+}$ and *AceCS2*$^{-/-}$ mice (Table S2). There was no significant change in plasma glucose or in NEFA and ketone body levels between *AceCS2*$^{+/+}$ and *AceCS2*$^{-/-}$ mice (Table S2). There was also no significant difference in the percentage of fat mass between fed *AceCS2*$^{-/-}$ and *AceCS2*$^{+/+}$ mice as assessed by dual-energy X-ray absorption (DEXA) (Table S2). However, plasma acetate was 5- to 10-fold higher in *AceCS2*$^{-/-}$ mice as compared to *AceCS2*$^{+/+}$ mice under both fed and fasted conditions (Figure 3C). These data indicate that acetate utilization is impaired in *AceCS2*$^{-/-}$ mice, implying that a deficit in extrahepatic acetate utilization causes fasting-induced hypothermia. Acetyl-CoA levels were decreased by 75% in fasted *AceCS2*$^{-/-}$ mice (Figure 3D). NADH and ATP levels in skeletal muscles of fasted *AceCS2*$^{-/-}$ mice were significantly reduced compared to those found in *AceCS2*$^{+/+}$ mice (Figures 3E and 3F). These data indicate that AceCS2 plays a pivotal role in supplying acetyl-CoA for ATP production during 48 hr of fasting. Oxygen consumption was significantly increased after 36 hr fasting, and locomotor activity was not reduced (Figures 3G and 3H).

The hypothermia in *AceCS2*$^{-/-}$ mice also differs from adaptive hypothermia in response to cold (Lowell and Spiegelman, 2000). Exposure of these *AceCS2*$^{-/-}$ mice to low temperature (4°C) did

Figure 3. *AceCS2*-Deficient Mice Exhibit Low Body Temperature and Reduced Exercise Capacity during Fasting

(A) Core temperature of male mice (12 weeks old) fed on normal chow diet was monitored after 48 hr fasting (*AceCS2*$^{+/+}$, n = 8; *AceCS2*$^{-/-}$, n = 7). *p < 0.05 compared to *AceCS2*$^{+/+}$.

(B) Relative mRNA expression levels of AceCS2 in BAT of male mice (12 weeks old, six to seven per genotype). **p < 0.01 compared to *AceCS2*$^{+/+}$.

(C) Plasma acetate levels of male mice (12 weeks old) fed or fasted for 48 hr (fed *AceCS2*$^{+/+}$, n = 4; fasted *AceCS2*$^{+/+}$, n = 4; fed *AceCS2*$^{-/-}$, n = 4; fasted *AceCS2*$^{-/-}$, n = 4).

(D) Acetyl-CoA levels in gastrocnemius muscle from 48 hr fasted male *AceCS2*$^{+/+}$ and *AceCS2*$^{-/-}$ mice (12 weeks old) were measured (*AceCS2*$^{+/+}$, n = 7; *AceCS2*$^{-/-}$, n = 8).

(E) ATP content is markedly reduced in *AceCS2*$^{-/-}$ mice. ATP and AMP contents of gastrocnemius muscle from male *AceCS2*$^{+/+}$ and *AceCS2*$^{-/-}$ mice were measured at 12 weeks of age (*AceCS2*$^{+/+}$, n = 7; *AceCS2*$^{-/-}$, n = 8). **p < 0.01 compared to *AceCS2*$^{+/+}$.

(F) NAD^+ and NADH levels and NAD^+/NADH ratio in gastrocnemius muscle and BAT of 48 hr fasted male *AceCS2*$^{+/+}$ and *AceCS2*$^{-/-}$ mice (12 weeks old) (*AceCS2*$^{+/+}$, n = 4; *AceCS2*$^{-/-}$, n = 4).

(G) Oxygen consumption (VO_2) (left panel), average of VO_2 (center panel), and RQ (respiratory quotient) (right panel) were determined in fasted male mice (12 weeks old) by indirect calorimetry (*AceCS2*$^{+/+}$, n = 6; *AceCS2*$^{-/-}$, n = 5).

(H) Total locomotor activity of male mice (14 weeks old) was measured by beam breaks in the light and dark periods (*AceCS2*$^{+/+}$, n = 12; *AceCS2*$^{-/-}$, n = 12).

(I) Male mice (12 weeks old) given food and water ad libitum were subjected to cold (4°C) (left panel) (*AceCS2*$^{+/+}$, n = 10; *AceCS2*$^{-/-}$, n = 11). Male mice (12 weeks old) fasted for 24 hr and given water ad libitum were subjected to cold (4°C) (right panel) (*AceCS2*$^{+/+}$, n = 7; *AceCS2*$^{-/-}$, n = 8). Core temperature was monitored over a 5 hr period.

(J) Male mice (12 weeks old, nine per genotype) were subjected to a run-to-exhaustion protocol on a motorized treadmill under fed conditions and 48 hr fasted conditions (*AceCS2*$^{+/+}$, n = 9; *AceCS2*$^{-/-}$, n = 9). *p < 0.05 compared to fed.

All values are mean ± SEM.

not further reduce their body temperatures under the fed condition (Figure 3I, left panel). We next examined the effect of cold exposure on 24 hr fasted mice. Unlike with 48 hr fasting, under 24 hr fasting conditions, *AceCS2*$^{-/-}$ mice maintained their core body temperatures at levels similar to *AceCS2*$^{+/+}$ mice, although both levels were equally reduced by 2°C–3°C compared to fed levels. Exposure of these mice to cold further decreased their core temperatures; however, after 5 hr cold exposure, there was no significant difference between *AceCS2*$^{-/-}$ and *AceCS2*$^{+/+}$ mice (Figure 3I, right panel). These data indicate that adaptive thermogenesis in response to low temperature was not impaired in *AceCS2*$^{-/-}$ mice and further suggest that the sympathetic nervous system is able to properly maintain core body temperature in *AceCS2*$^{-/-}$ mice.

We hypothesized that fasting *AceCS2*$^{-/-}$ mice would lead to decreased exercise tolerance, owing to impaired acetate oxidation and subsequent reduction of ATP production in skeletal muscle (Figure 3E). *AceCS2*$^{-/-}$ mice were exercised on a motorized treadmill apparatus using a run-to-exhaustion protocol. *AceCS2*$^{-/-}$ mice fasted for 48 hr exhibited a markedly reduced capacity to sustain running exercise, whereas the running capacity of *AceCS2*$^{+/+}$ mice did not change between the fed and fasted conditions (Figure 3J). This suggests that acetate is an important fuel required for exercise as well as for heat generation during fasting.

AceCS2$^{-/-}$ Mice Compensate for Metabolic Acidosis through Hyperventilation

Because the plasma acetate levels are very high in *AceCS2*$^{-/-}$ mice, we speculated that these mice could be acidotic, and, if not, they might be hyperventilating to blow off CO_2 to prevent acidemia. Accordingly, we measured the arterial blood gases, pH, and bicarbonate concentration. The values of arterial carbon dioxide partial pressure ($PaCO_2$) were significantly decreased in *AceCS2*$^{-/-}$ mice ($p < 0.05$, n = 5–6), indicating that *AceCS2*$^{-/-}$ mice were hyperventilating to blow off CO_2. There were no significant differences in the values of PaO_2, standardized bicarbonate concentration ($[HCO_3^-]$), and the pH (Table 1). These data indicate that *AceCS2*$^{-/-}$ mice were hyperventilating to compensate for a possible acidosis caused by acetate accumulation. This hyperventilation in *AceCS2*$^{-/-}$ mice might account for some of their increased energy expenditure compared to *AceCS2*$^{+/+}$ mice.

AceCS2$^{-/-}$ Mice Exhibit Hypothermia and Hypoglycemia under Low-Carbohydrate, High-Fat Diet

Similar to fasting conditions, we hypothesized that acetate utilization may be important under low-glucose or low-carbohydrate intake states. To examine this possibility, 4-week-old *AceCS2*$^{-/-}$ and *AceCS2*$^{+/+}$ mice were fed a low-carbohydrate, high-fat diet (LC/HF; 0.4% carbohydrate, 90.5% fat, and 9.1% protein from calories). At the time of weaning (4 weeks of age), *AceCS2*$^{-/-}$ mice weighed an average of 40% less than their littermates (Figures S1A–S1C), and plasma acetate levels were markedly elevated (Figure 4A). Plasma ketone bodies, NEFA, glucose, and insulin levels were comparable between *AceCS2*$^{+/+}$ and *AceCS2*$^{-/-}$ mice (Table S1).

On LC/HF diet, *AceCS2*$^{-/-}$ mice exhibited lower body temperatures (Figure 4B). This was most severe (30.1 ± 1.4°C) on day 2 of LC/HF diet feeding, whereas *AceCS2*$^{+/+}$ mice maintained their body temperatures at 37°C on this diet. In addition, *AceCS2*$^{-/-}$ mice lost weight, whereas the body weight of *AceCS2*$^{+/+}$ mice remained stable (Figure 4C). Furthermore, *AceCS2*$^{-/-}$ mice had sustained hypoglycemia (56 ± 5 mg/dl) over this period compared to *AceCS2*$^{+/+}$ mice that exhibited transiently decreased plasma glucose levels at weaning but soon recovered to normal levels (137 ± 7 mg/dl) (Figure 4D). This transient hypoglycemia in *AceCS2*$^{+/+}$ is most likely from the stress of forced weaning, which causes suppression of feeding on the day of weaning. Plasma NEFA and ketone body levels were highly elevated, but there were no significant differences between *AceCS2*$^{+/+}$ and *AceCS2*$^{-/-}$ mice except in ketone body levels on day 3 of the LC/HF diet (Figures 4E and 4F). The abundance of mRNAs for the enzymes involved in gluconeogenesis was not decreased in *AceCS2*$^{-/-}$ mice compared to *AceCS2*$^{+/+}$ mice (Figure S3A). Furthermore, injection of pyruvate to these mice rescued hypoglycemia (Figure S3B), indicating that the gluconeogenic pathway is intact.

Table 1. Blood Gas Analysis of *AceCS2*$^{+/+}$ and *AceCS2*$^{-/-}$ Mice

	+/+	−/−
pH	7.34 ± 0.03	7.34 ± 0.03
PaO_2 (mm Hg)	102.3 ± 2.7	108.8 ± 5.5
$PaCO_2$ (mm Hg)	37.3 ± 1.2	33.3 ± 0.9[a]
HCO_3^- (mM)	19.7 ± 0.8	17.6 ± 1.3
BE (mM)	−5.1 ± 1.2	−6.9 ± 1.9

Male mice (12 weeks old, n = 6 per genotype) were fed on a normal chow diet. Samples were obtained from the femoral artery of awake, freely moving mice. Data are mean ± SEM.
[a] $p < 0.05$ compared to *AceCS2*$^{+/+}$.

After 5 days of LC/HF diet feeding, *AceCS2*$^{-/-}$ mice began to die, and, by 21 days, 50% of the *AceCS2*$^{-/-}$ mice had died. By contrast, none of *AceCS2*$^{+/+}$ mice died (Figure 4G). However, following 21 days on the LC/HF diet, the surviving *AceCS2*$^{-/-}$ mice gradually recovered body temperature and plasma glucose levels. We observed no further excess mortality (data not shown).

Weight, body temperature, and plasma parameters (glucose, NEFA, and ketone bodies) did not differ significantly between the *AceCS2*$^{-/-}$ mice that died and those that survived during the 4 day period of LC/HF feeding after the weaning (Figures S4A–S4E). Therefore, the cause of death was not simply from malnutrition. We also examined the effect of a high-carbohydrate, high-fat (HC/HF) diet (58% fat, 15% protein, and 27% carbohydrate from calories). On this diet, both *AceCS2*$^{-/-}$ and *AceCS2*$^{+/+}$ mice survived with no deaths (data not shown). These data indicated that acetate oxidation mediated by AceCS2 is essential to maintain normal thermogenesis and fuel usage under low-glucose utilization states such as low-carbohydrate diets or fasting.

AceCS2$^{-/-}$ Mice Exhibit Low Body Weight Gain under Low Carbohydrate Intake

We continued to feed the surviving *AceCS2*$^{-/-}$ mice an LC/HF diet. *AceCS2*$^{+/+}$ mice fed on this diet gained weight efficiently; by contrast, *AceCS2*$^{-/-}$ mice exhibited reduced weight gain under this diet (Figure 5A). Food intake was unchanged between

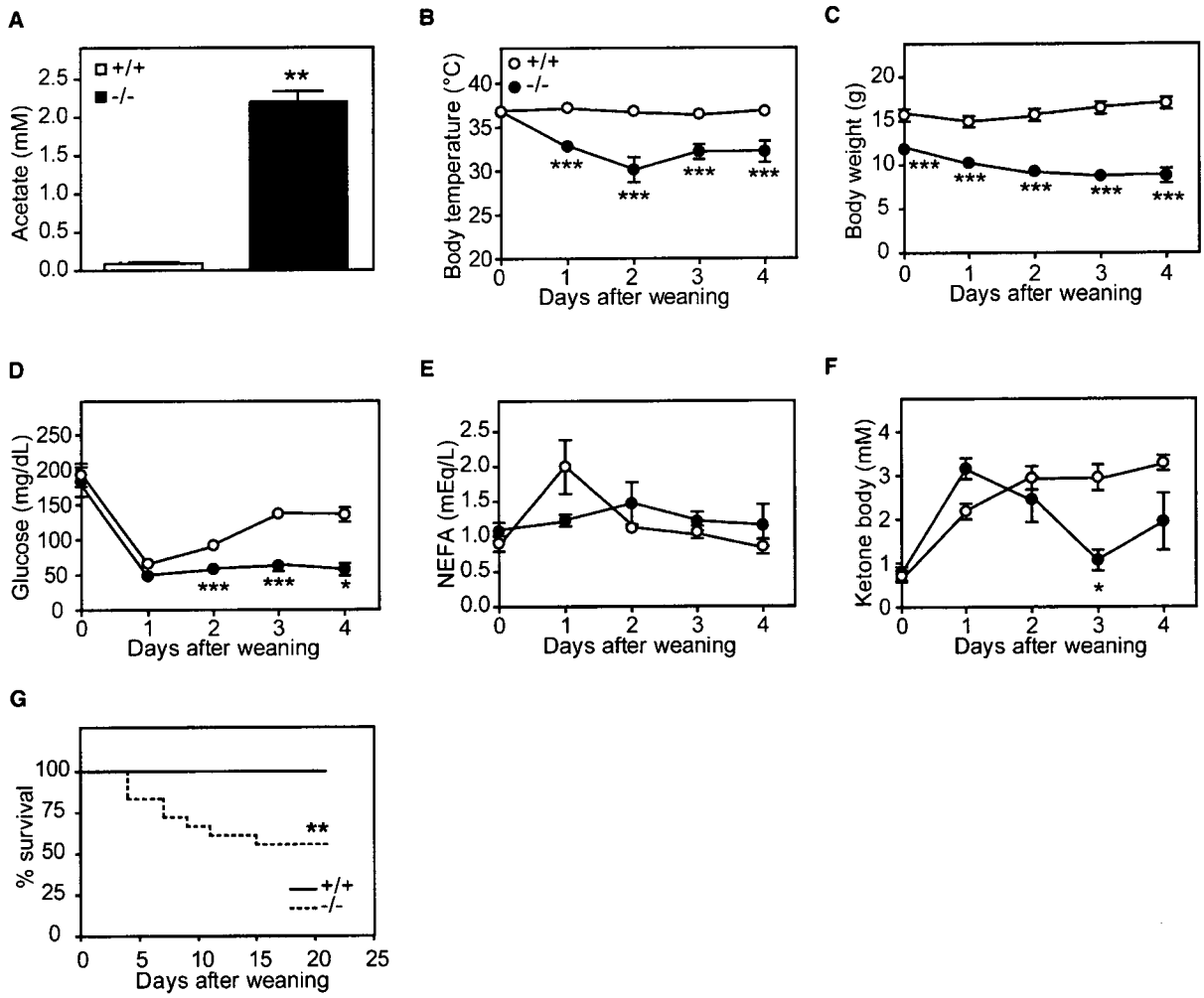

Figure 4. *AceCS2*-Deficient Mice Exhibit Hypothermia When Fed an LC/HF Diet

(A) Male mice (4 weeks old, five per genotype) were fed milk from their mother. Plasma acetate levels were measured.

(B–F) Male mice (4 weeks old) were fed an LC/HF diet. (B) Core rectal temperature, (C) body weight, (D) blood glucose, (E) plasma NEFA, and (F) plasma ketone body level were measured (*AceCS2*$^{+/+}$, n = 8; *AceCS2*$^{-/-}$, n = 7). *p < 0.05, **p < 0.01, and ***p < 0.001 compared to *AceCS2*$^{+/+}$.

(G) Kaplan-Meier analysis of survival in males fed an LC/HF diet at 4 weeks old (*AceCS2*$^{+/+}$, n = 22; *AceCS2*$^{-/-}$, n = 18). **p < 0.001 compared to *AceCS2*$^{+/+}$ by Log-rank test. Data are mean ± SEM.

AceCS2$^{+/+}$ and *AceCS2*$^{-/-}$ mice (Figure 5B). We excised various tissues from these mice and measured tissue weights. The photo shown in Figure 5C was taken for representative mice of each group. There were no marked differences in the weights of liver, kidney, BAT, and heart between *AceCS2*$^{+/+}$ and *AceCS2*$^{-/-}$ mice, but the fat pads of *AceCS2*$^{-/-}$ mice were significantly smaller than those of *AceCS2*$^{+/+}$ mice (Figure 5D). We measured metabolic parameters of these mice at 24 weeks of age (Table 2). Although the plasma glucose levels were unchanged, plasma insulin levels decreased significantly in *AceCS2*$^{-/-}$ mice as compared to *AceCS2*$^{+/+}$ mice. Plasma levels of leptin were 4-fold lower, but plasma acetate was 7-fold higher in *AceCS2*$^{-/-}$ mice (Table 2).

In order to investigate the mechanism underlying reduced weight gain in *AceCS2*$^{-/-}$ mice, food intake and energy expenditure were examined. *AceCS2*$^{-/-}$ mice exhibited consistently higher rates of oxygen consumption and, therefore, had higher metabolic rates than *AceCS2*$^{+/+}$ mice throughout day and night (Figure 5E). After adjusting for allometric scaling and gender, the effect of the *AceCS2*$^{-/-}$ allele was highly significant ($p < 0.01$, n = 7, multiple ANOVA) (Figure 5E, right panel). The respiratory quotient was 0.71 in both *AceCS2*$^{+/+}$ and *AceCS2*$^{-/-}$ mice (data not shown). These data suggested that the resistance to weight gain of *AceCS2*$^{-/-}$ mice may be, at least in part, due to increased energy expenditure. To examine the possibility that fatty acids synthesis is changed in *AceCS2*$^{-/-}$ mice, we measured malonyl-CoA levels and acetyl-CoA carboxylase (ACC) activity (Figure S5). Malonyl-CoA levels and ACC activity in skeletal muscle and BAT did not significantly differ between *AceCS2*$^{-/-}$ and *AceCS2*$^{+/+}$ mice (Figure S5). In liver, malonyl-CoA levels

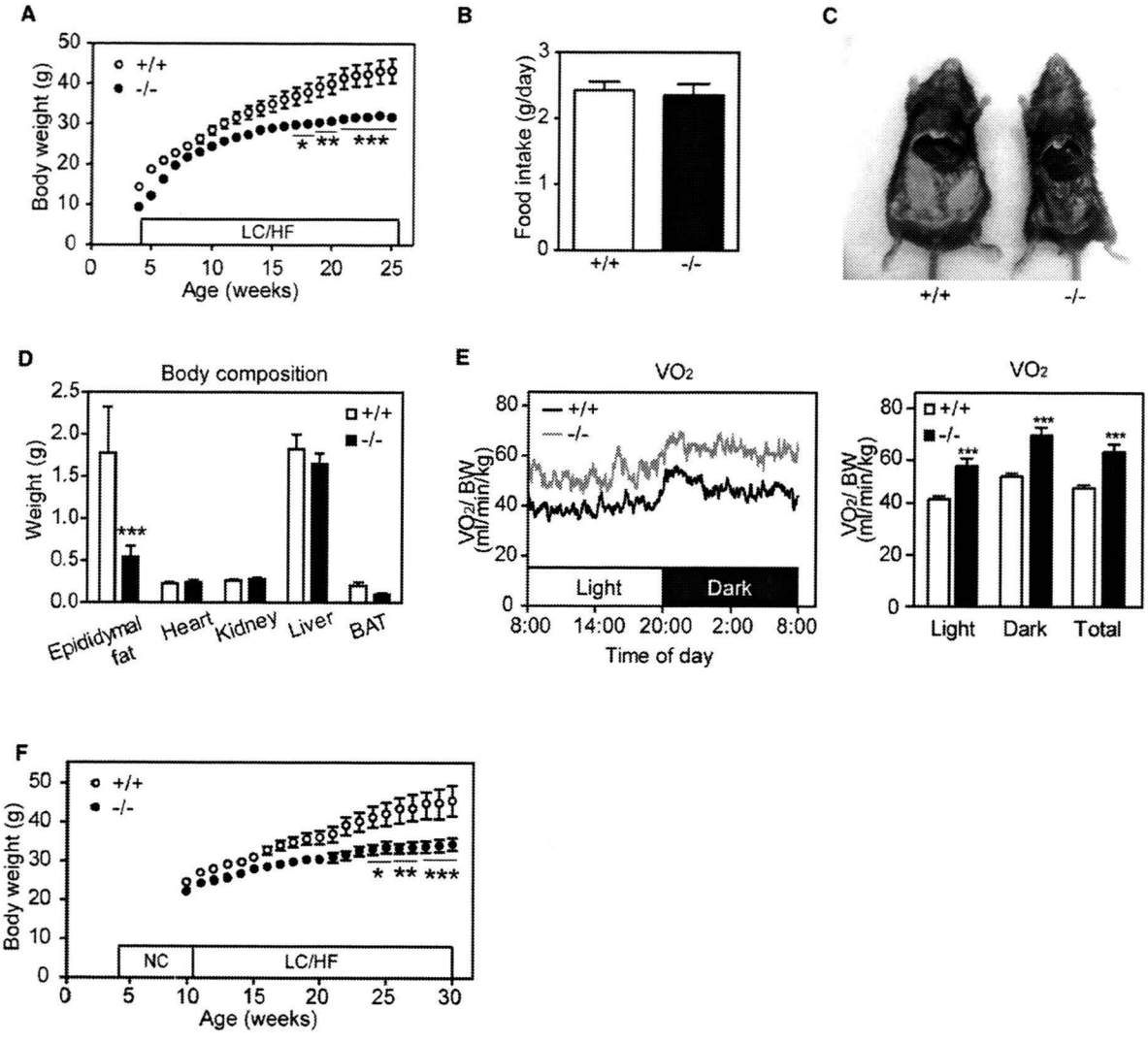

Figure 5. *AceCS2* Deficiency Attenuates Body Weight Gain in Mice Fed an LC/HF Diet

(A) Body weight change of male mice fed an LC/HF diet from 4 weeks old (*AceCS2*$^{+/+}$, n = 15; *AceCS2*$^{-/-}$, n = 12).

(B) Food intake of male mice fed an LC/HF diet at 25 weeks old (*AceCS2*$^{+/+}$, n = 15; *AceCS2*$^{-/-}$, n = 12).

(C) Representative picture of *AceCS2*$^{+/+}$ and *AceCS2*$^{-/-}$ male mice (26 weeks of age) fed an LC/HF diet.

(D) Various tissue weights for *AceCS2*$^{+/+}$ and *AceCS2*$^{-/-}$ male mice (26 weeks of age) fed an LC/HF diet (*AceCS* $^{+/+}$, n = 5; *AceCS2*$^{-/-}$, n = 5).

(E) Oxygen consumption (VO_2, left panel) and average of VO_2 (right panel) were determined in male mice (26 weeks old) fed an LC/HF diet by indirect calorimetry (*AceCS2*$^{+/+}$, n = 8; *AceCS2*$^{-/-}$, n = 7). Data are corrected for body weight. The original, uncorrected data are shown in Figure S6.

(F) Change of body weight. Male mice were weaned at 4 weeks and were fed on normal chow diet for 6 weeks (until 10 weeks of age) and switched to an LC/HF diet (*AceCS2*$^{+/+}$, n = 8; *AceCS2*$^{-/-}$, n = 8). *p < 0.05, **p < 0.01, and ***p < 0.001 compared to *AceCS2*$^{+/+}$. Data are mean ± SEM. NC, normal chow diet.

were reduced by 20% in *AceCS2*$^{-/-}$ (Figure S5), which could be the secondary effect of lower plasma insulin levels since AceCS2 is not expressed in liver. These data suggested that fatty acid synthesis and degradation are not impaired by the deficiency of *AceCS2*.

It is possible that the reduced weight gain of *AceCS2*$^{-/-}$ mice during LC/HF diet feeding simply resulted from a failure to thrive phenotype (reduced body weight gain, hypothermia, hypoglycemia, and low survival rate) induced by low-carbohydrate diet feeding immediately after weaning (Figure 4). Therefore, after weaning, we first fed the mice a normal chow diet for 6 weeks (until 10 weeks of age) and then switched them to an LC/HF diet. By contrast to feeding an LC/HF diet immediately after weaning, none of these *AceCS2*$^{-/-}$ mice died; however, they did exhibit reduced weight gain compared to *AceCS2*$^{+/+}$ mice following the switch to an LC/HF diet (Figure 5F). Reduced weight gain was observed only under a low-carbohydrate regimen. When mice were fed a high-fat, high-carbohydrate diet, *AceCS2*$^{-/-}$ mice were not protected against weight gain (data not shown). These results clearly indicate that adult

Table 2. Metabolic Parameters of *AceCS2*$^{-/-}$ and *AceCS2*$^{+/+}$ Mice Fed an LC/HF Diet

	+/+	−/−
Glucose (mg/dl)	233 ± 14	233 ± 22
Cholesterol (mg/dl)	110 ± 7	70 ± 11[b]
Triglycerides (mg/dl)	93 ± 6	92 ± 9
NEFA (μEql/l)	343 ± 17	332 ± 71
Ketone body (mM)	0.387 ± 0.064	0.705 ± 0.116[a]
Leptin (ng/ml)	2.80 ± 1.12	0.74 ± 1.03[b]
Insulin (ng/ml)	3.34 ± 1.3	1.54 ± 0.71[a]
Acetate (mM)	0.18 ± 0.06	0.97 ± 0.17[b]

Male mice (24 weeks old, seven to nine per genotype) were fed an LC/HF diet. Assays of blood samples were performed on isolated plasma.
[a] $p < 0.05$.
[b] $p < 0.01$ compared to *AceCS2*$^{+/+}$.

AceCS2$^{-/-}$ mice exhibit reduced adiposity under high-fat feeding, low-carbohydrate intake, or ketogenic conditions.

DISCUSSION

Under ketogenic conditions, free fatty acids are released into the circulation and taken up by thermogenic tissues such as BAT and skeletal muscle, where they serve as a fuel for thermogenesis (Picard et al., 2002; Spiegelman and Flier, 2001). Fatty acids are also taken up by liver for the generation of ketone bodies, and these ketone bodies are subsequently utilized in extrahepatic tissues. In addition, previous studies showed that an appreciable amount of acetate is generated in liver and this acetate can subsequently be utilized by extrahepatic tissues (Leighton et al., 1989; Murthy and Steiner, 1973; Seufert et al., 1974). Here, we demonstrate that acetate also serves as a fuel that has specific functions that do not overlap with those of fatty acids and ketone bodies in thermogenesis.

Our studies of mice with targeted deletion of *AceCS2* reveal that these animals can not maintain normal body temperature when starved or when fed an LC/HF diet. Under these conditions, *AceCS2*$^{-/-}$ mice display sustained hypoglycemia, strongly diminished capacity for exercise, and dramatically increased mortality as compared to their wild-type or heterozygous littermates. The mutant animals also exhibit strikingly reduced rates of whole-body acetate oxidation and correspondingly increased levels of acetate in plasma. Most importantly, ATP levels in the skeletal muscle of 48 hr fasted *AceCS2*$^{-/-}$ mice were profoundly reduced, showing the significant contribution of acetate and AceCS2 to the energy supply under ketogenic conditions. Therefore, under ketogenic conditions, the hypothermia and poor exercise tolerance observed in the *AceCS2*$^{-/-}$ mice is most likely from a lack of acetate utilization as a fuel source. Supporting this possibility, plasma acetate levels were significantly higher under fasting conditions than under fed conditions. This suggests that acetate turnover is significantly higher in the fasted state primarily due to AceCS2.

LC/HF diet has been generally recognized to have weight-reducing effects on obese animals (Kennedy et al., 2007). Although the body weight gain of mice fed an LC/HF diet is significantly lower than that of those fed high-fat and high-carbohydrate diets, our LC/HF diet has no weight-reducing or anti-weight-gaining effect. In the experiments done by Kennedy et al. (2007), 8-week-old mice fed a normal chow diet were switched to an LC/HF diet, and the weight of mice fed an LC/HF diet dropped until it stabilized at 85% of the initial weight. The discrepancy between these results may result from the difference in the composition of the different LC/HF diets. The LC/HF diet that Kennedy et al. used consists of 78.85% fat, 9.5% protein, and 0.76% carbohydrate, whereas our LC/HF diet (purchased from Harlan Teklad) contains 67.4% fat, 15.3% protein, and 0.6% carbohydrate (% by weight). In addition, the source of the fat is also different. The LC/HF diet in their study contains lard and butter, whereas our LC/HF diet contains vegetable shortening. Regardless of the differences in the exact diet, we show that AceCS2 is critical for normal body weight gain under an LC/HF diet.

Recent observations indirectly support a role for *AceCS2* as a determinant of growth and adiposity. From the mapping of a quantitative trait locus (QTL) region on mouse chromosome 2 that has a large effect on growth and adiposity, AceCS2 was reported as 1 of 18 candidate genes potentially controlling predisposition to growth and predisposition to obesity (Jerez-Timaure et al., 2005).

Although plasma acetate is very high in *AceCS2*$^{-/-}$ mice, we found that there was appropriate and sufficient respiratory compensation for any metabolic acidosis caused by acetate accumulation. *AceCS2*$^{-/-}$ mice exhibited hypocapnea to maintain a neutral arterial blood pH. Patients with chronic obstructive lung disease and cystic fibrosis commonly have low body weight, which is believed to be related to inadequate energy intake, nutrient malabsorption, and excessive energy expenditure (Bell et al., 1996). Basal metabolic rate is 10%–20% greater in these patients than in healthy subjects and may contribute to their energy imbalance. Furthermore, increased oxygen consumption caused by increased respiratory muscle activity has been reported in these patients, which largely explains the increased basal metabolic rate (Campbell et al., 1959; Cherniack, 1959; Donahoe et al., 1989; McGregor and Becklake, 1961). Because *AceCS2*$^{-/-}$ mice seem to be hyperventilating, this increased use of respiratory muscles might account for, at least in part, the higher oxygen consumption.

We previously identified AceCS2 as a target of KLF15 (Yamamoto et al., 2004). The fasting-induced transcription of AceCS2 is largely dependent on KLF15. Similarly to *AceCS2*$^{-/-}$ mice, KLF15-deficient mice also exhibit severe hypoglycemia after overnight fasting (Fisch et al., 2007). KLF15 plays an important role in gluconeogenesis by regulating amino acid degradation and key gluconeogenic enzymes such as phosphoenolpyruvate carboxykinase in the liver during fasting (Gray et al., 2007; Teshigawara et al., 2005). Our data indicate that KLF15 is crucial for survival during starvation through two mechanisms: (1) gluconeogenesis in liver and (2) acetate oxidation to generate ATP and heat in muscle and BAT through AceCS2 activity.

The sirtuins comprise a conserved family of proteins that are believed to mediate some of the health benefits of calorie restriction, which leads to extension of life span in nearly all organisms studied, including mammals. SIRT1 has been reported to function as an energy-sensing gene that senses NAD^+ levels and regulates the activity of critical transcriptional regulators of

metabolism in multiple tissues (Yang et al., 2007). Within the mitochondria, SIRT3 deacetylates a key lysine residue on AceCS2, leading to its enzymatic activation (Hallows et al., 2006; Schwer et al., 2006; Schwer and Verdin, 2008). As SIRT3 protein levels are specifically increased in calorie-restricted mammals, regulation of AceCS2 activity by SIRT3 could be a key metabolic factor responsible for homeostatic regulation during calorie restriction, leading to its positive effect on life span. Sirt3 was recently shown to be necessary for maintaining basal ATP levels with ATP levels in multiple organs of *Sirt3*$^{-/-}$ mice that are markedly reduced compared to wild-type levels (Ahn et al., 2008). This study, along with ours, suggests that activation of AceCS2 by Sirt3 is required to maintain basal ATP levels in mammals. Future studies of AceCS2- and AceCS2-deficient mice are warranted to investigate this potentially exciting link between longevity and mitochondrial energy metabolism.

In conclusion, our current findings demonstrate that acetate metabolism mediated by AceCS2 is crucial for survival and energy production under ketogenic conditions such as starvation or diabetes. These and future studies of acetate metabolism mediated by AceCS2 will have a significant impact on the understanding of the acetate metabolism for heat generation and energy metabolism.

EXPERIMENTAL PROCEDURES

Generation of AceCS2-Deficient Mice

We constructed a targeting plasmid by using genomic DNA fragments derived from Sv129 mice. A Lac Z and a neomycin cassette flanked by two loxP sites were introduced into the *AceCS2* locus of ES cells (derived from the Sv129 strain). Electroporation, selection, and screening were performed with standard gene-targeting techniques. Briefly, genomic DNA was isolated from neomycin-resistant ES cell clones, digested with KpnI, and subjected to hybridization with a probe to detect homologous recombination and the presence of the flox allele (Figure 1A).

Chimeric males were generated by using the morula aggregation technique and mated to C57BL/6J female mice. Homologous recombination was confirmed by Southern blotting (Figure 1B). Deletion of RNA transcripts and protein was confirmed by QRT-PCR and western blotting, respectively (Figures 1D and 1E). After achieving germline transmission, *AceCS2*$^{+/-}$ mice were crossed with C57BL/6J for six to nine generations.

Heterozygous mice were mated to obtain *AceCS2*$^{-/-}$ mice. Wild-type littermates were used as controls throughout the study. Genotyping of mice used in this study was performed by PCR of tail DNA as shown in Figure 1C; the mutant allele was detected by using a pair of oligonucleotides (5′-GGCGCACAA CAAAACCTAGT-3′ and 5′-GACAGTATCGGCCTCAGGAA-3′) that amplify a 512 bp PCR product between the *AceCS2* and sequence 3′ to *Lac Z/neo* cassette. The wild-type allele was detected by PCR with a pair of oligonucleotides (5′-GGCGCACAACAAAACCTAGT-3′ and 5′-GGGGTTCGTGCCTGGTTG-3′) that amplify a 355 bp PCR product spanning exon 1.

Quantitative Real-Time PCR

Quantitative real-time PCR (QRT-PCR) was performed as previously described (Tanaka et al., 2003). All primer sequences used in this paper are available upon request.

Antibody

To produce rabbit polyclonal anti-murine AceCS2 (IgGA001), a 12-residue peptide corresponding to the C terminus of murine AceCS2 (CQKYEEQ RAATN) was synthesized (Sigma Genesis, Japan), coupled to keyhole limpet hemocyanin, and injected into New Zealand White rabbits. IgG fractions were prepared by affinity chromatography on protein A-Sepharose (GE Healthcare Bioscience). For immunoblot analysis, an aliquot of whole-cell lysates from heart (20 μg) was subjected to SDS-PAGE on 10% gels followed by analysis with a 1:1000 dilution of anti-AceCS2 (Fujino et al., 2001).

Animal Experiments

All procedures were performed in accordance with Japanese Physiological Society guidelines for animal care. Mice were group housed in cages with a 12 hr light/12 hr dark cycle and fed a standard rodent chow diet (CE-2; CLEA Japan, Osaka). To induce a ketogenic condition, we compared an LC/HF diet (Table S3; Rho et al., 1999) (TD96355; Harlan Teklad Premier Laboratory Diets) consisting of 90.5% fat, 9.1% protein, and 0.4% carbohydrate (0% sucrose from calories) to a high-carbohydrate, high-fat diet consisting of 58.0% fat, 15.0% protein, and 27.01% carbohydrate from calories (Tanaka et al., 2003). All mice had free access to water. Food consumption was monitored daily, and body weight was recorded every week, unless otherwise stated.

Core body temperature was monitored using a rectal thermometer at 10 a.m. For the exercise performance, the mice were trained on the treadmill (MK-680AT/02M, Muromachikikai, Tokyo) prior to the exercise performance test (a 10 min run at 10 m/min at a 5° incline once per day for 4 days). Exhaustion was defined as the point at which mice were unable to continue running.

Food Intake, Locomotor Activity, and Metabolic Rate Measurement

Male mice (26 weeks old) were housed under controlled lighting (12 hr light-dark cycle) and temperature (23°C) conditions. Food (standard chow pellets or an LC/HF diet) and water were available ad libitum. Mice were then housed singly under the same conditions as above for an acclimation period of at least 7 days. Body weights and food intake were monitored daily for the duration of the study. Energy expenditure was measured by indirect calorimetry as described previously (MK-5000RQ; Muromachi, Tokyo) (Takayasu et al., 2006). Mice were placed in the calorimeter chambers and acclimated for 1 day. Locomotor activity was measured by using an infrared (IR) passive sensor system as described previously (Supermex, Muromachi Kikai, Japan) (Takayasu et al., 2006). The experiment was started at 8 a.m. (light period).

Acetate Oxidation

Acetate ([1-^{14}C]acetate, CFA13, GE Healthcare UK Limited) oxidation was measured in vivo as described (Wolfgang et al., 2006). The in vivo rate of ^{14}C-acetate oxidation (2 μCi [1 Ci = 37 GBq] of [1-^{14}C]acetate injected intraperitoneally) to $^{14}CO_2$ was determined after treatment of mice. Mice were acclimated in metabolic chambers fitted with 2-aminoethanol traps to recover expired $^{14}CO_2$. The oxidation of [1-^{14}C]acetate to form $^{14}CO_2$ was measured at 20 min intervals over the next 1 hr. At the end of experiment, plasma was collected, and plasma [1-^{14}C]acetate was measured.

Acetate Measurement

Plasma acetate levels were measured as described by (Hillman et al. 1978) with slight modifications. Briefly, plasma was mixed with 1 mM isovaleric acid as the internal standard. The sample was acidified with one-fifth the volume of 10% sulfosalicylic acid and then extracted three times with 10 volumes of diethylether. The ether extract was immediately back extracted into 0.2 M NaOH. The ether was removed under a stream of dry nitrogen. Before injection, the sample was reacidified with one-fifth the volume of 10% phosphoric acid. The acetate concentration of the sample was analyzed by gas chromatograph (GC-2014, Shimadzu, Japan) equipped with a flame ionization detector and a capillary column (ULBON HR-20 M, 0.25 mm i.d. × 25 m × 0.25 μm). The column was operated at 140°C. The injection port and the flame ionization detector were maintained at 300°C. The chromatograph was standardized with a mixture of C2-C7 short-chain fatty acids.

Plasma Parameters

Mice were sacrificed by CO_2 asphyxiation following a 4 hr fast during the light cycle (food removed 9:00 a.m., sacrificed at 1:00 p.m.). Blood was drawn by cardiac puncture, and the plasma was separated immediately by centrifugation and stored at −80°C until use. Plasma glucose, NEFA, triglycerides, total cholesterol, and total ketone body levels were determined by Glucose C2-test (Wako Pure Chemical, Japan), NEFA C-test (Wako Pure Chemical, Japan), Triglyceride E-test (Wako Pure Chemical, Japan), Cholesterol E-test (Wako Pure Chemical, Japan), and Autokit Total Ketone Bodies (Wako Pure

Chemical, Japan), respectively. Plasma insulin and leptin levels were determined by ELISA with an insulin immunoassay kit (Shibayagi, Japan) and a mouse leptin immunoassay (R & D systems) according to the manufacturer's instructions.

Assay Procedure for Acetyl-CoA, Adenine Nucleotides, NAD$^+$, and NADH Contents

Acetyl-CoA and adenine nucleotide contents in skeletal muscle or BAT of 12-week-old male mice were measured essentially as described previously (Miura et al., 2006; Scott et al., 1992; Takamura et al., 1985). NAD$^+$ and NADH nucleotide concentrations were directly measured by NAD$^+$/NADH Assay kit (Biochain Institute, Inc.) according to the manufacturer's instructions. The detail methods are described in the Supplemental Experimental Procedures.

Blood Gas Analysis

Blood gas analysis was performed as previously described (Kuwaki et al., 1996). A catheter was implanted into the right femoral artery under isoflurane (2%–3%) anesthesia. Up to 70 μl of arterial blood was drawn from the indwelling catheter after a recovery period of more than 2 hr and when the animal was quietly awake. Blood gases were determined by a blood gas analyzer (ABL500, Radiometer, Copenhagen).

Statistical Analyses

All values are expressed as mean ± standard error of the mean unless otherwise specified. Significant differences between mean values were evaluated using two-tailed, unpaired Student's t test (when two groups were analyzed) or one-way ANOVA followed by Student Newman-Keuls test (for three or more groups).

SUPPLEMENTAL DATA

Supplemental Data include Supplemental Experimental Procedures, six figures, and three tables and can be found with this article online at: http://www.cell.com/cell-metabolism/supplemental/S1550-4131(08)00393-8.

ACKNOWLEDGMENTS

We thank Dr. Rob Rawson for critical reading of the manuscript; Drs. Peter Edwards and Mitsuhiro Watanabe for helpful discussions; and Kaori Ikeda, Junko Kuno, Satomi Takahashi, Yuko Kai, and Mika Nomiyama for technical assistance. This work was supported through ERATO JST, NIBIO by the NFAT project of the NEDO and by the Special Coordination Fund for Science and Technology from the Ministry of Education, Culture, Sports, Science, and Technology. This work was also supported, in part, by Astellas Foundation for Research on Metabolic Disorders, the Uehara Memorial Foundation, and the Ono Medical Foundation. M.Y. is an Investigator of the Howard Hughes Medical Institute. J.S. is an Investigator of Translational Systems Biology and Medicine Initiative (TSBMI).

Received: June 6, 2008
Revised: October 15, 2008
Accepted: December 12, 2008
Published: February 3, 2009

REFERENCES

Ahn, B.H., Kim, H.S., Song, S., Lee, I.H., Liu, J., Vassilopoulos, A., Deng, C.X., and Finkel, T. (2008). A role for the mitochondrial deacetylase Sirt3 in regulating energy homeostasis. Proc. Natl. Acad. Sci. USA *105*, 14447–14452.

Bell, S.C., Saunders, M.J., Elborn, J.S., and Shale, D.J. (1996). Resting energy expenditure and oxygen cost of breathing in patients with cystic fibrosis. Thorax *51*, 126–131.

Campbell, E.J., Westlake, E.K., and Cherniack, R.M. (1959). The oxygen consumption and efficiency of the respiratory muscles of young male subjects. Clin. Sci. (Lond.) *18*, 55–64.

Cherniack, R.M. (1959). The oxygen consumption and efficiency of the respiratory muscles in health and emphysema. J. Clin. Invest. *38*, 494–499.

Donahoe, M., Rogers, R.M., Wilson, D.O., and Pennock, B.E. (1989). Oxygen consumption of the respiratory muscles in normal and in malnourished patients with chronic obstructive pulmonary disease. Am. Rev. Respir. Dis. *140*, 385–391.

Fisch, S., Gray, S., Heymans, S., Haldar, S.M., Wang, B., Pfister, O., Cui, L., Kumar, A., Lin, Z., Sen-Banerjee, S., et al. (2007). Kruppel-like factor 15 is a regulator of cardiomyocyte hypertrophy. Proc. Natl. Acad. Sci. USA *104*, 7074–7079.

Fujino, T., Kondo, J., Ishikawa, M., Morikawa, K., and Yamamoto, T.T. (2001). Acetyl-CoA synthetase 2, a mitochondrial matrix enzyme involved in the oxidation of acetate. J. Biol. Chem. *276*, 11420–11426.

Fukao, T., Lopaschuk, G.D., and Mitchell, G.A. (2004). Pathways and control of ketone body metabolism: On the fringe of lipid biochemistry. Prostaglandins Leukot. Essent. Fatty Acids *70*, 243–251.

Gray, S., Wang, B., Orihuela, Y., Hong, E.G., Fisch, S., Haldar, S., Cline, G.W., Kim, J.K., Peroni, O.D., Kahn, B.B., et al. (2007). Regulation of gluconeogenesis by Kruppel-like factor 15. Cell Metab. *5*, 305–312.

Hallows, W.C., Lee, S., and Denu, J.M. (2006). Sirtuins deacetylate and activate mammalian acetyl-CoA synthetases. Proc. Natl. Acad. Sci. USA *103*, 10230–10235.

Hillman, R.E. (1978). Simple, rapid method for determination of propionic acid and other short-chain fatty acids in serum. Clin. Chem. *24*, 800–803.

Ikeda, Y., Yamamoto, J., Okamura, M., Fujino, T., Takahashi, S., Takeuchi, K., Osborne, T.F., Yamamoto, T.T., Ito, S., and Sakai, J. (2001). Transcriptional regulation of the murine acetyl-CoA synthetase 1 gene through multiple clustered binding sites for sterol regulatory element-binding proteins and a single neighboring site for Sp1. J. Biol. Chem. *276*, 34259–34269.

Jerez-Timaure, N.C., Eisen, E.J., and Pomp, D. (2005). Fine mapping of a QTL region with large effects on growth and fatness on mouse chromosome 2. Physiol. Genomics *21*, 411–422.

Kennedy, A.R., Pissios, P., Otu, H., Xue, B., Asakura, K., Furukawa, N., Marino, F.E., Liu, F.F., Kahn, B.B., Libermann, T.A., et al. (2007). A high-fat, ketogenic diet induces a unique metabolic state in mice. Am. J. Physiol. Endocrinol. Metab. *292*, E1724–E1739.

Kuwaki, T., Cao, W.H., Kurihara, Y., Kurihara, H., Ling, G.Y., Onodera, M., Ju, K.H., Yazaki, Y., and Kumada, M. (1996). Impaired ventilatory responses to hypoxia and hypercapnia in mutant mice deficient in endothelin-1. Am. J. Physiol. *270*, R1279–R1286.

Leighton, F., Bergseth, S., Rortveit, T., Christiansen, E.N., and Bremer, J. (1989). Free acetate production by rat hepatocytes during peroxisomal fatty acid and dicarboxylic acid oxidation. J. Biol. Chem. *264*, 10347–10350.

Lowell, B.B., and Spiegelman, B.M. (2000). Towards a molecular understanding of adaptive thermogenesis. Nature *404*, 652–660.

Luong, A., Hannah, V.C., Brown, M.S., and Goldstein, J.L. (2000). Molecular characterization of human acetyl-CoA synthetase, an enzyme regulated by sterol regulatory element-binding proteins. J. Biol. Chem. *275*, 26458–26466.

Matthias, A., Ohlson, K.B., Fredriksson, J.M., Jacobsson, A., Nedergaard, J., and Cannon, B. (2000). Thermogenic responses in brown fat cells are fully UCP1-dependent. UCP2 or UCP3 do not substitute for UCP1 in adrenergically or fatty scid-induced thermogenesis. J. Biol. Chem. *275*, 25073–25081.

McGregor, M., and Becklake, M.R. (1961). The relationship of oxygen cost of breathing to respiratory mechanical work and respiratory force. J. Clin. Invest. *40*, 971–980.

Miura, S., Tomitsuka, E., Kamei, Y., Yamazaki, T., Kai, Y., Tamura, M., Kita, K., Nishino, I., and Ezaki, O. (2006). Overexpression of peroxisome proliferator-activated receptor gamma co-activator-1alpha leads to muscle atrophy with depletion of ATP. Am. J. Pathol. *169*, 1129–1139.

Murthy, V.K., and Steiner, G. (1973). Hepatic acetate levels in relation to altered lipid metabolism. Metabolism *22*, 81–84.

Picard, F., Gehin, M., Annicotte, J., Rocchi, S., Champy, M.F., O'Malley, B.W., Chambon, P., and Auwerx, J. (2002). SRC-1 and TIF2 control energy balance between white and brown adipose tissues. Cell *111*, 931–941.